GCAGS JOURNAL
A Publication of the Gulf Coast Association of Geological Societies
www.gcags.org

# Zircon U–Pb Geochronology and Sources of Volcanic Ash Beds in the Upper Cretaceous Eagle Ford Shale, South Texas

**John D. Pierce[1,2], Stephen C. Ruppel[1], Harry Rowe[2], and Daniel F. Stockli[3]**

[1]*Bureau of Economic Geology, Jackson School of Geosciences, University of Texas at Austin, 10100 Burnet Rd., Austin, Texas 78758, U.S.A.*

[2]*Chevron Corporation, 1400 Smith St., Houston, Texas 77002, U.S.A.*

[3]*Department of Geological Sciences, University of Texas at Austin, 1 University Station C1100, Austin, Texas 78712, U.S.A.*

## ABSTRACT

**The Eagle Ford Shale and equivalent Boquillas Formation (Late Cretaceous) contain abundant volcanic ash beds of varying thickness. These ash beds represent a unique facies that displays a range of sedimentary structures, bed continuity, and diagenetic alteration. They are prominent not only in West Texas outcrops, but also in the subsurface of South Texas where hydrocarbon exploration and production is active. Additionally, the ash beds have potential for stratigraphic correlation and most importantly for obtaining high-resolution geochronology, which can then be used for defining depositional rates, chronostratigraphy, and facies architecture.**

**Ash beds were sampled from outcrops in West Texas, subsurface cores in Central Texas, and at near surface exposures in Austin, Texas. The ash beds were collected throughout the entirety of the Eagle Ford succession and ranged in thickness from 0.05–13 inches. The ash beds contained high amounts of non-detrital zircons that were dated using U–Pb. High-resolution ages were obtained by laser ablation analysis of zircons collected from ash beds at the base and top of the Eagle Ford, as well as at the Cenomanian-Turonian boundary. U–Pb ages indicate the Eagle Ford in West Texas ranges in age from early Cenomanian (96.8 Ma +1.2/-0.7 Ma) to early Coniacian (87.1 ± 0.3 Ma), a duration of about 9.7 Ma. By contrast, the top of the succession in the Austin area extends only to the late Turonian (91.6 +0.6/-0.4 Ma). Ash bed ages from subsurface cores define the base of the Eagle Ford to be, at least locally, much younger than observed elsewhere (94.66 ± 0.36 Ma) which can be attributed to the development of significant precursor topography at the beginning of the Eagle Ford transgression. Dates for the Cenomanian-Turonian boundary interval are consistent with those defined in previous studies.**

**X-ray fluorescence (XRF) and diffraction (XRD), radiometrics, and rare earth element (REE) analysis of ash beds were combined with knowledge of paleowind that suggests likely sources of the ash beds are from arc volcanoes in northern and central Mexico and proximal volcanoes in Central Texas from the Balcones Igneous Province. This study is the first detailed regional analysis of the age, geochemistry, and source of the ash beds in the Eagle Ford Shale and equivalent Boquillas Formation. As such, it provides key insights into the age and duration of this system, serves as a basis for better interpretations of facies interrelationships, and places constraints on the interpretation of biostratigraphic and chemostratigraphic indicators of temporal relationships throughout the region.**

## INTRODUCTION

The Eagle Ford Shale is one of the largest active unconventional reservoirs in the United States. Its time of deposition overlaps the notable Oceanic Anoxic Event II (OAE II) and the Cenomanian-Turonian (C–T) boundary (Phelps, 2011; Fairbanks, 2012; Denne et al., 2014). Much of the OAE II and C–T boundary research undertaken to date in North America has focused on strata deposited north of the Eagle Ford in the Western Interior Seaway (Fig. 1) (e.g., Elder, 1987, 1991; Kirkland, 1991; Obradovich, 1993; Kennedy et al., 2005; Meyers, et al., 2012), with only recent studies having begun to identify this event and boundary in the Eagle Ford (e.g., Denne et al., 2014). While the OAE II is present in the Eagle Ford, it has not yet received the same level of attention as the Global Boundary Stratotype Section Point (GSSP) in Pueblo, Colorado (e.g., Leckie et al., 2002;



Manuscript received March 30, 2016; revised manuscript received June 13, 2016; manuscript accepted June 29, 2016.

GCAGS Journal, v. 5 (2016), p. 253–274.

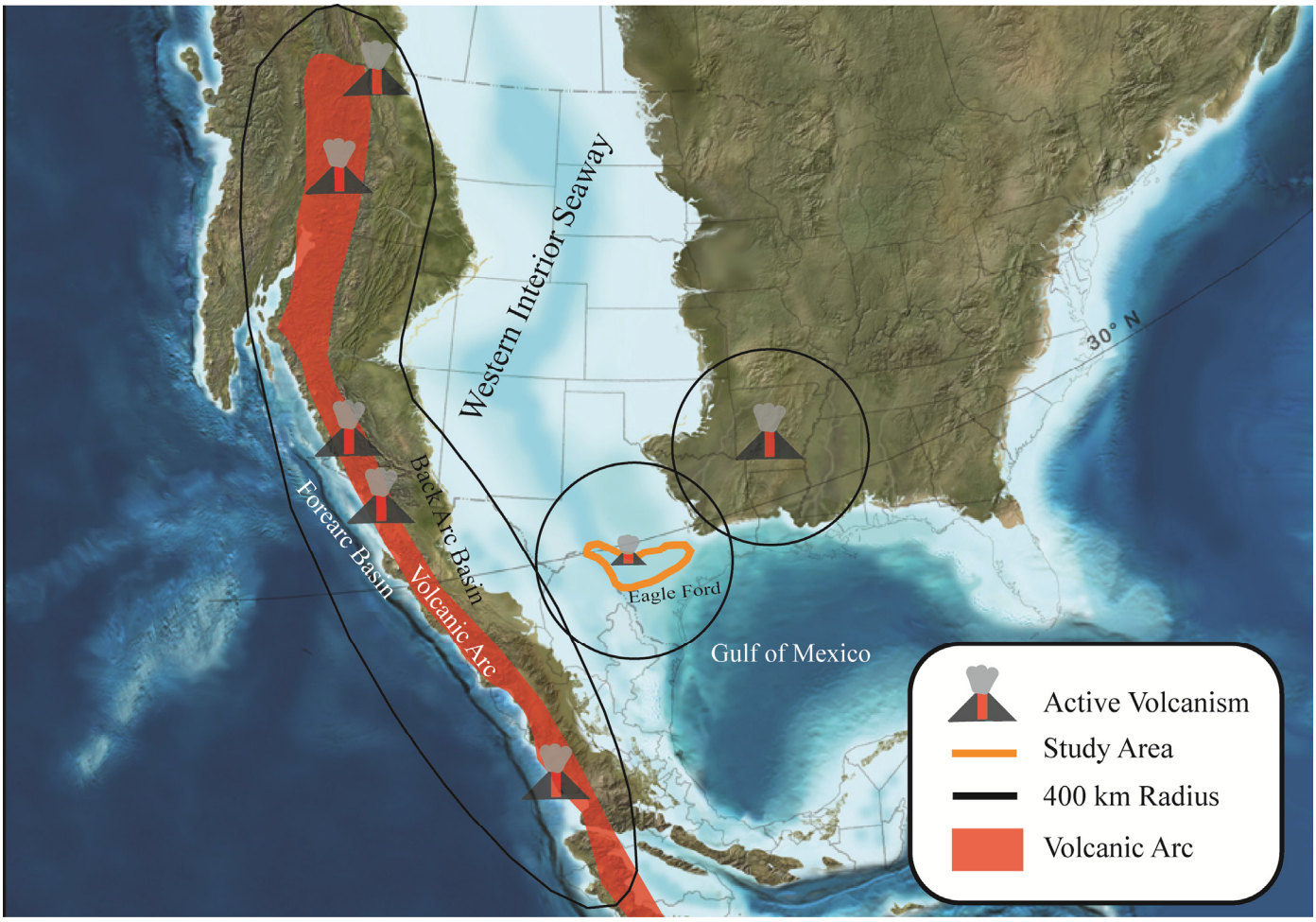


**Figure 1. Paleogeography of North America during Turonian time (modified after Blakey, 2013). Known areas of active volcanism during Eagle Ford deposition are indicated by volcano symbols. Active volcanoes are known from Washington, Oregon, Arkansas, Texas; Canada; and Sonora and Zihuatanejo, Mexico (Ross et al., 1929; Stott, 1963; Baldwin and Adams, 1971; Gill and Coban, 1973; Armstrong et al., 1977; Hunter and Davies, 1979; Ewing and Caren, 1982; Elder, 1988; Silver et al., 1993; Cardin et al., 1995; McDowell et al., 2001; Centeno-Garcia et al., 2008).**

Erba, 2004; Meyers et al., 2012; Sageman et al., 2014; Ma et al., 2014). Recent research in planktonic biostratigraphy and radioisotopic geochronology from the Eagle Ford permits a more complete comparison with previous studies from the Western Interior Seaway than previously deemed possible (Harbor, 2010; Corbett and Watkins, 2013; Denne et al., 2014; Eldrett et al., 2014, 2015a; Fairbanks et al., 2016; Frebourg et al., 2016).

Like the strata in the Western Interior Seaway, the Eagle Ford contains abundant volcanic ash beds throughout much of its distribution. Ash beds are prominent in West Texas outcrops, as well as in subsurface cores where hydrocarbon production and exploration is active. These rocks display a variety of sedimentary structures, bed continuity, diagenetic alteration, and thicknesses ranging from 0.05–13 inches. Although the continuity of these ash beds has not been demonstrated, the beds have been used as tools by oil and gas geologists for local and regional correlation. We present the first detailed study of these ash beds, their origin, ages of deposition, and chemistry, to provide a greater understanding of the regional facies architecture of the Eagle Ford Shale.

This study comprises three main components. First, the study provides the first regional chronostratigraphic framework for the Eagle Ford based on U–Pb geochronology of zircons using laser ablation inductively coupled mass spectrometry (LA–ICP–MS). The study is the first to incorporate radioisotopic ages across the basin, and provide a regional context for recent local geochronological studies by Eldrett et al. (2014, 2015a, 2015b). Second, the study examines potential volcanic source(s) for the numerous ash accumulations during Eagle Ford time (Fig. 1). Integrating findings from bulk major element ash chemistry, trace and rare earth elements, mineralogy, and visual inspection of phenocrysts and trace minerals from mineral separates provides the potential to identify the source region(s). Third, the study integrates U–Pb ages with existing biostratigraphic studies in each of the three sample locations. This integration provides a unique opportunity to directly assign radioisotopic ages to biostratigraphic boundaries, thus providing an unequivocal correlation method and eliminating long-range lithostratigraphic correlations that are common with the work done in the Western Interior Seaway. In order to better relate the three localities, the new ages presented herein for the C–T boundary in South Texas Eagle Ford strata are integrated with published results and interpretations developed from studies of the GSSP.

## GEOLOGIC SETTING

The Upper Cretaceous (Cenomanian-Coniacian) Eagle Ford (Fig. 2) is a regionally extensive, carbonate- and organic-rich mudrock that extends 400 miles from the Rio Grande Embayment, near the Texas-Mexico border to the East Texas Basin (Hentz and Ruppel, 2010). The Eagle Ford is a mixed siliciclastic/carbonate system with primary sediment accumulation con-

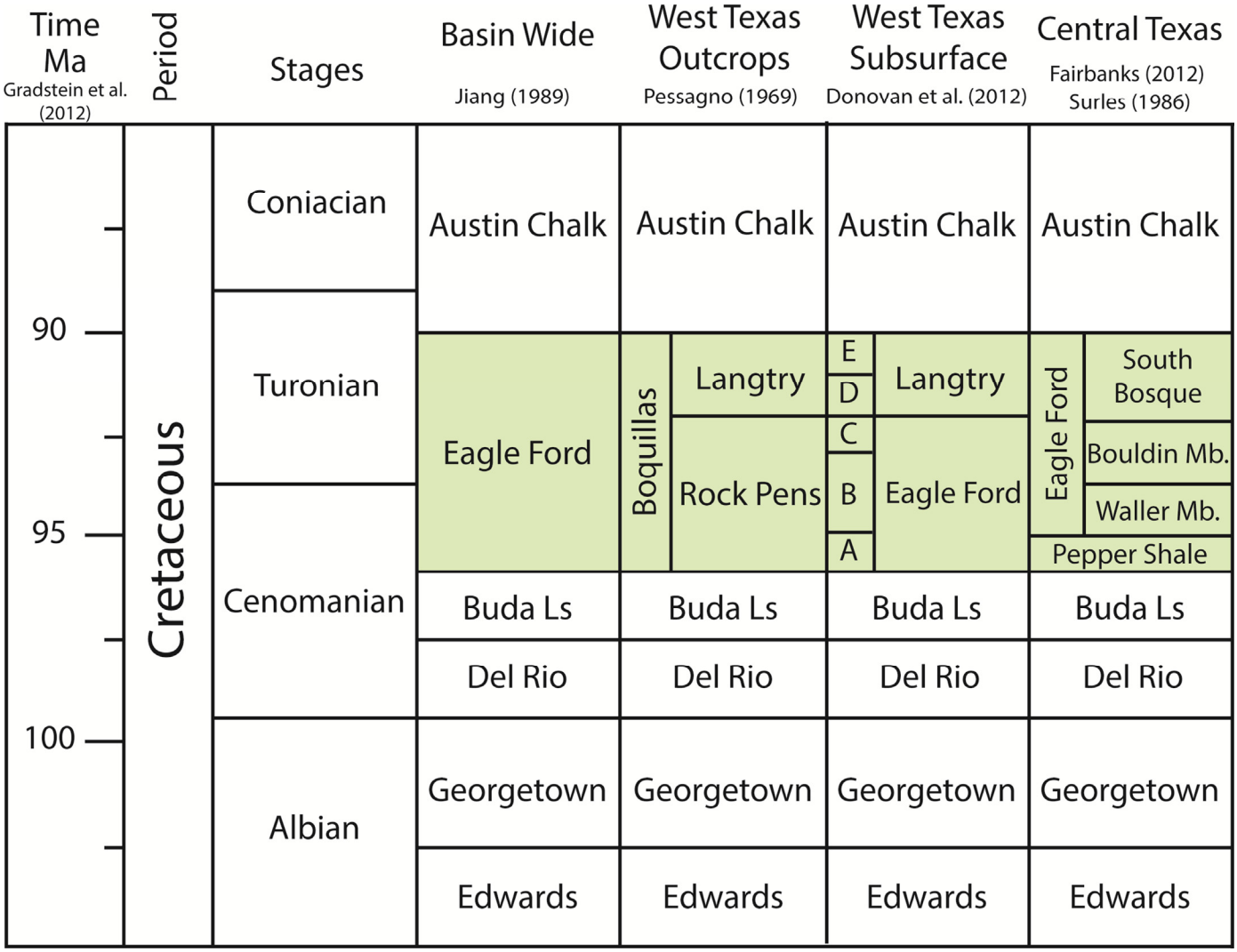


**Figure 2. Regional stratigraphic column of Albian through Coniacian units across South Texas (modified after Pessagno, 1969; Surles, 1986; Jiang, 1989; Donovan et al., 2012; Fairbanks, 2012).**

centrated on the Comanchean Shelf beginning in the early-Cenomanian (Galloway, 2008). In the East Texas Basin, the Eagle Ford is primarily a siliciclastic-dominated system due to influence from the Woodbine Delta to the east, while west of the San Marcos Arch, the Eagle Ford becomes a more carbonate-dominated system due to greater distance from Woodbine delta sediments (Fig. 3). The stratigraphic thickness of the Eagle Ford varies greatly from approximately 40 feet along the San Marcos Arch to more than 400 feet in the Maverick Basin (Hentz and Ruppel, 2010). Regional thickening is observed to the west in the Maverick Basin due to increased rates of subsidence (Hentz and Ruppel, 2010).

The Buda Formation—a regionally extensive, burrowed, lime-wackestone with low but variable clay mineral content—unconformably underlies the Eagle Ford (Fig. 2). It is composed of three members interpreted to be a transgressive-regressive depositional cycle (Hazzard, 1959; Donovan et al., 2010). Using isopachs of the Buda, Hentz and Ruppel (2010) demonstrated that regional thickening is apparent across the Maverick Basin. This shows that differential subsidence continued into Eagle Ford time, while thinning is observed across the San Marcos Arch.

The Eagle Ford represents a time of maximum transgression across the Comanchean shelf. Basal beds of the Eagle Ford prominently incorporate rip up clasts of Buda origin (Ruppel et al., 2013). Varying nomenclature has been applied to the Eagle Ford based upon location (Fig. 2). This study follows the convention of Donovan et al. (2012), dividing the Eagle Ford into upper and lower intervals, as well as referring to the Eagle Ford west of the Pecos Rivers as the Boquillas Formation (Fig. 2). This division is observable through the subsurface and are correlatable through a sharp spectral gamma decrease (specifically U concentration) from the lower Eagle Ford to the upper Eagle Ford with an accompanying sharp drop in Mo content (Donovan et al., 2012, Eldrett et al., 2014). Specifically, this division separates organic-rich, argillaceous lower Eagle Ford from the higher oxygenated, lower-gamma, upper Eagle Ford. Further division of the upper and lower Eagle Ford was proposed by Donovan and Staerker (2010), dividing the Eagle Ford into five subunits (A–E) at the Lozier Canyon outcrop (Figs. 2 and 3). East of the San Marcos Arch, the Eagle Ford is broken down into the Pepper Shale, Waller Member, Bouldin Member, and South Bosque Formation (Fig. 2) (Surles, 1986; Fairbanks, et al., 2016).

Overlying the Eagle Ford is the Austin Chalk (Fig. 2), a highly bioturbated lime mudstone composed primarily of planktonic foraminifera, calcispheres, and coccoliths (Ruppel et al., 2013). In the West Texas outcrops, as well as in the subsurface, the contact between the Eagle Ford and the lime wackestones of the Austin Chalk appears to be gradational (Harbor, 2010; Fry, 2015). However, in the East Texas Basin, the Sabine Uplift resulted in erosion of Eagle Ford strata causing a depositional hia-

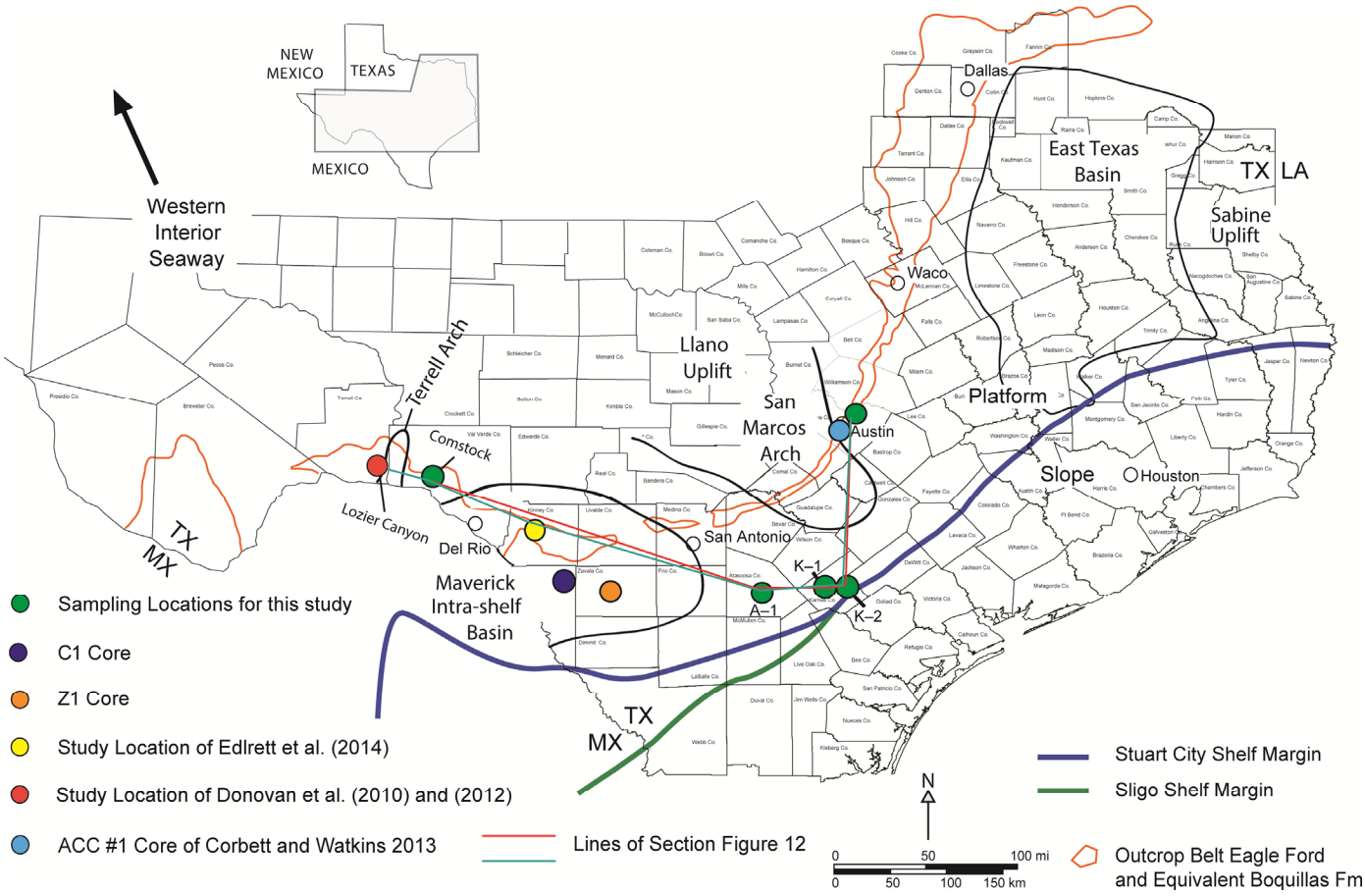


**Figure 3. Regional map of Texas with locations of this study (from Ruppel et al., 2012, courtesy of the Texas Bureau of Economic Geology).**

tus prior to Austin Chalk deposition (Mancini and Puckett, 2005). The relative age of the boundary in West Texas has conflicting results. Using nanoplankton biostratigraphy, Donovan et al., (2012) (Fig. 3) defined the contact to be of late Coniacian age in Lozier Canyon. In contrast, Cobban et al. (2008) placed the base of the Austin Chalk in Lozier Canyon near the Turonian-Coniacian boundary using inoceramid molluscs.

## METHODS

### Sampling

A total of 14 ash beds were collected from three locations covering the major stratigraphic levels within the Eagle Ford/Boquillas and parts of the Austin Chalk: 6 ash beds collected at surface exposures near Comstock in West Texas, 5 ash beds collected from subsurface cores from Atascosa and Karnes counties, Texas, and 3e ash beds collected from a surface pit in Austin, in Central Texas (Fig. 3). Outcrop ash bed samples were selected from ash beds 2 inches and thicker to collect sufficient sample, roughly 4 kilograms, and ensuring greater quantities of datable zircons. Ash layers characterized by moderate-to-severe bottom current reworking were not sampled to reduce the possibility of introducing detrital zircons. Given the high specific gravity of zircons (4.85 grams per cubic centimeter), sampling efforts were focused on the basal portion of the ash as differential settling may have occurred as the ashes were deposited in water. In outcrops, ash beds were identified by their recessive nature and high clay content in relation to the surrounding shales and calcareous packstones (Fig. 4). Ash beds collected from subsurface cores were identified by their fluorescence under ultraviolet light. Sample selection was limited in the 4 inch diameter cores to thicker ash beds. In order to recover enough zircons for LA–ICP–MS dating, selected ash beds were a minimum of 3 inches thick.

### U–Pb Geochronology

Due to the high clay mineral content in most ash bed samples, traditional sample preparation was insufficient and ineffective. A complete and detailed procedure of modified mineral separation is found in Table 1. A total of 985 individual zircon crystals from the 14 samples were dated in order to provide a regional, temporal framework of deposition, and paleoceanographic changes across the broad South Texas shelf (Eagle Ford–Austin Chalk transition). Samples displayed varying abundances of zircon crystals with 17 and 164 representing the minimum and maximum range of zircons analyzed in a sample. While the variation in zircon abundance is large between some samples, zircon abundances in most samples were sufficient to evaluate an average of 55 to 65 single crystals per sample. The crystals were individually picked under binocular microscope and mounted on double-sided tape in preparation for laser ablation. The selection process of the zircons included careful examination of the crystals' exterior morphology, avoiding crystals with obvious fractures, large fluid inclusions that could not be avoided during ablation, and fragmented and incomplete crystals.

### U–Pb Source of Error and Uncertainty

Single crystal analytical uncertainties calculated from LA–ICP–MS are typically less than 1.0%, ultimately limited by

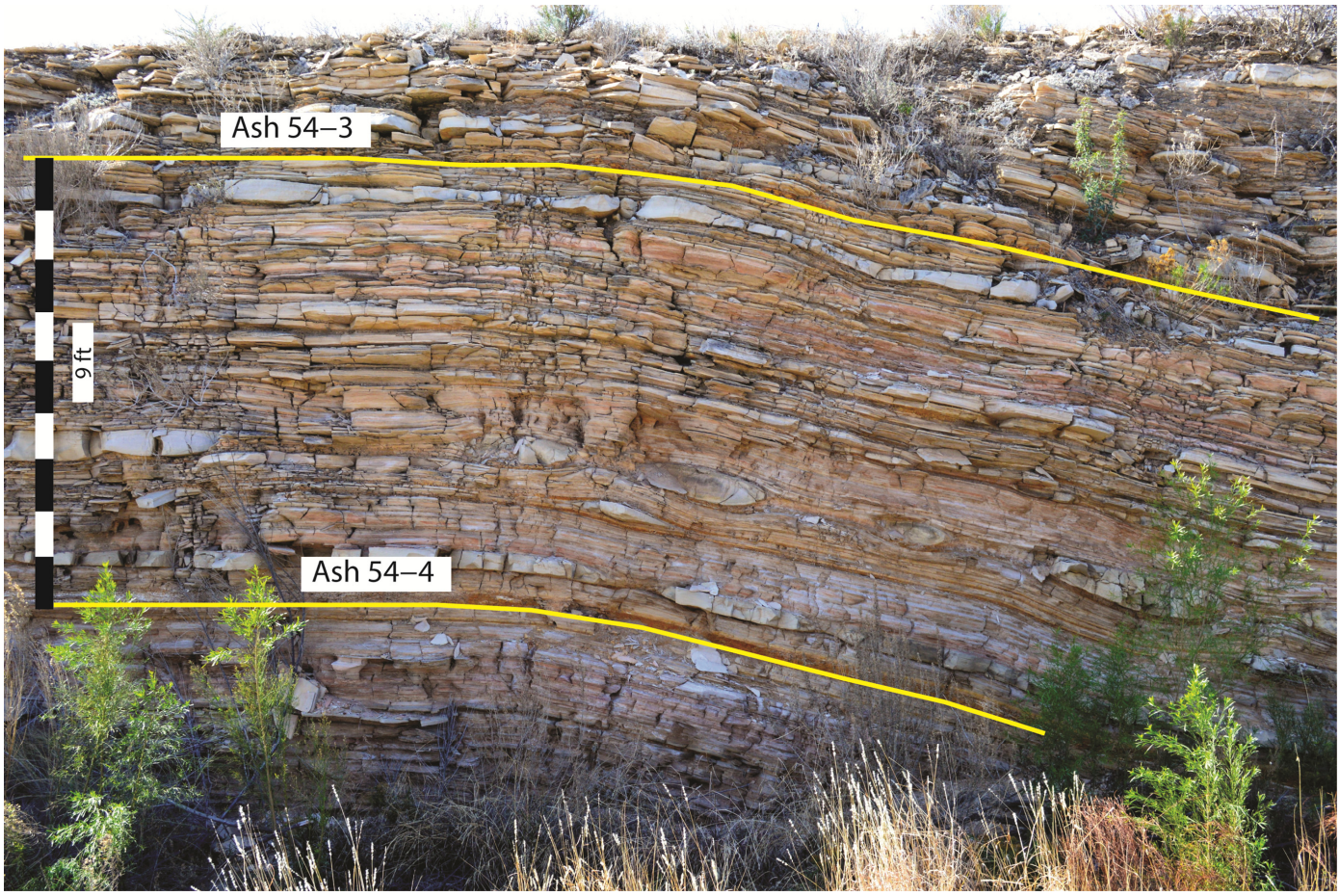


**Figure 4. Photograph of outcrop section 54 located near Comstock, Texas. Locations of ash bed samples 54–4 and 54–3 are shown. Ashes can be easily identified by their recessive nature in outcrop, as well as their tendency to be white, red, and purple in color.**

**Table 1. A detailed step by step guide of the mineral separation process. Due to the high clay mineral content of many of the samples, traditional methods of mineral separations were found to be inadequate, thus a revised method was devised.**

| | |
|---|---|
| Step 1 | Crushing and grinding in a jaw crusher and disk mill were ineffective with the sticky, swelling ash beds. To overcome this problem, jaw-crushed samples were soaked in water and dish detergent for a 48 hour period. |
| Step 2 | Once soaked, the samples generally disaggregated sufficiently to be wet sieved through a series of three mesh sizes: 250, 100, and 45 micron openings. |
| Step 3 | Zircons possessing a diameter of less than 45 microns are not suitable for LA–ICP–MS, due to the spot size of the laser (~30 microns) and were discarded. |
| Step 4 | Between the processing of each sample, mesh screens were thoroughly washed and run through a sonic bath to discharge all grains from the screen. |
| Step 5 | The 45 to 100 micron fraction of the sample was subsequently dried and processed through a Frantz magnetic separator using three separate settings. |
| Step 6 | The parameters for the first round consisted of a 0.75 Ampere current with a slide slope of 7 degrees. The parameters for the next two rounds consisted of a 1.25 Ampere current with a slope of 5 degrees. Parameters for the concluding round consisted of a 2 Ampere current with a slope of 2 degrees. |
| Step 7 | After each round of magnetic separation, the non-magnetic and magnetic fraction was visually inspected using short wave ultraviolet light. If noticeable zircons were present in the magnetic fraction, the process would restart at a lower initial current and steeper slope. |
| Step 8 | The non-magnetic fraction yielding zircons was then processed through heavy liquids separation. Outcrop samples were processed through lithium metatungstate (LMT) (2.8 grams per milliliter) for 24 hours in order to allow enough settling time of the zircon grains through the viscous heavy liquid. |
| Step 9 | Samples from Austin and the subsurface were processed through both bromoform (2.89 grams per milliliter) and methylene iodide (3.22 grams per milliliter). The use of bromoform and methylene iodide was used due to lower densities, allowing for a more consistent mineral separation. |

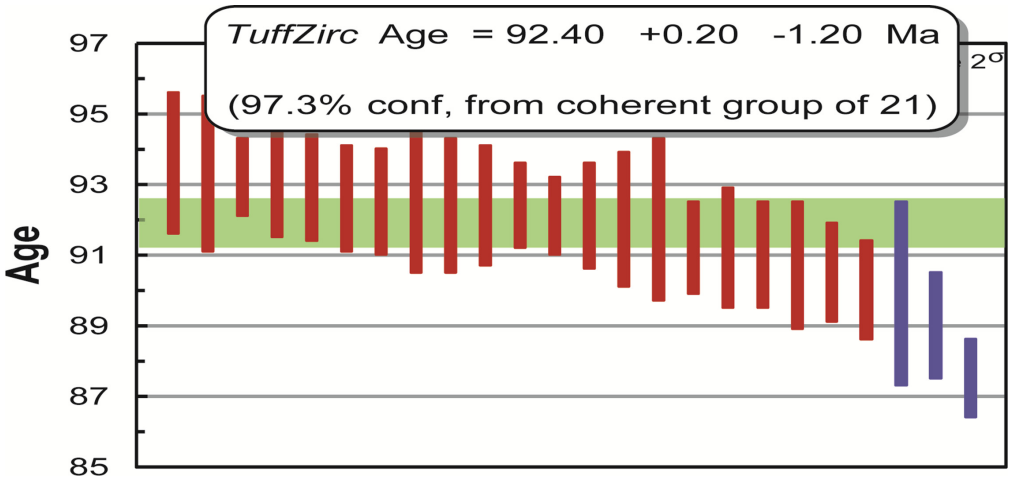


**Figure 5. Tera-Wasserburg plot (Tera and Wasserburg, 1972) for ash bed sample 42–1, Comstock, Texas (Fig. 8). These plots were used to easily identify samples with common Pb and/or Pb loss so they could be eliminated from the final coherent group used to calculate the eruptive age. Error ellipses are 2σ for each single crystal. TuffZirc age displays the calculated $^{206}Pb/^{238}U$ age with red bars indicating grains used in the coherent group. Blue bars represent sample grains that were dropped from the calculation due to Pb loss or inheritance.**

standard variability seen in the lab standard reference zircon GJ–1 (Horstwood, 2008; Sylvester, 2008). While LA–ICP–MS does not provide the same level of precision as isotope dilution thermal ionization mass spectrometry (ID–TIMS), the high precision of ID–TIMS was deemed unnecessary for a large-scale regional study. Instead, using laser ablation provided large datasets in short periods of time and at a fraction of the cost, allowing for thorough analysis of many ash beds and thus the complexity of the zircon population(s). Eagle Ford zircon populations can be highly complex with a large range of crystallization ages. The range can be partially attributed to protracted crystallization histories in the magma chamber (Schoene et al., 2010); however, these are difficult to refine. The spread observed in individual crystals within an ash bed are too large to be completely attributed to long crystallization histories, indicating that Pb loss, xenocrystic zircons, and common Pb are contributing factors to the age ranges and spread of the data. This is confirmed by the depth-dependent ablation signal observed in the ablation process.

Zircons with results greater than 10% discordance were eliminated from the weighted mean calculations, as well as grains with high amounts of U and Th, as these contained the most Pb loss. In addition, common Pb was monitored and zones with high common Pb were excluded from the single crystal ages as part of the data reduction process by comparing the $^{207}Pb/^{206}Pb$ vs. $^{206}Pb/^{238}U$ ages. Zircons affected by more than 50% common Pb were eliminated entirely from calculations. Because common Pb was an issue with many samples, all data were graphed on Tera-Wasserburg plots (Fig. 5) to accurately display the single crystal ages and graphically eliminate and correct for common Pb (Tera and Wasserburg, 1972). Crystals with obvious xenocrysts were also eliminated from further analysis.

This iterative approach to data analysis and careful interpretation is necessary for determining a final eruption age from a complex suite of single crystal dates. All ages stated in this study are $^{206}Pb/^{238}U$ ages. For 12 samples, $^{206}Pb/^{238}U$ weighted mean ages were determined using TuffZirc from the ISOPLOT program (Ludwig, 1991). In these samples, a coherent group of crystals was selected to calculate the weighted mean with smallest variance, excluding grains with interpreted Pb loss and inheritance. The two remaining samples (unit E and A1–C2B11) were also calculated using TuffZirc; however, a large population of crystals that indicated Pb loss was included into the weighted mean, yielding an apparently younger age. In order to correct for this artifact, a coherent group was manually selected at the expense of increasing the variance, but yielding a more representative eruptive age. All crystal ages were calibrated against the GJ–1 zircon standard with an age of 601.7 ± 1.3 Ma as a primary reference material (Jackson et al., 2004).

## Geochemical Analysis

Geochemical analyses were carried out on 18 ash samples (Table 2) at all three study locations to better understand variations in chemical composition and the degree of diagenesis, and to fingerprint likely source areas. SGS Mineral Services carried out sodium peroxide fusion inductively coupled plasma atomic emission spectroscopy (ICP–AES) and ICP mass spectrometry (ICP–MS) analyses for 55 elements, and borate fusion X-ray fluorescence (XRF) of 13 major element oxides. REE abundances and calculations were determined using ICP–AES and ICP–MS data on trace elements. Complete suites of XRF major and trace elements were compiled for the A1, K1, K2, Z1, and C1 cores by the Mudrocks Systems Research Laboratory (MSRL) at the University of Texas at Austin using a Bruker handheld energy dispersive XRF (ED–XRF) scanner (Rowe et al., 2012). Additionally, X-ray diffraction (XRD) analysis of bulk sample and clay separates was completed by KT Geosciences of Gunnison, Colorado.

# RESULTS

## Eagle Ford Ash Bed Description, Mineralogy, and Elemental Geochemistry

### Volcanic Ash Bed Description

Volcanic ash beds within the Eagle Ford are easily identifiable. Individual ash beds vary greatly in abundance and thickness. In cores from Zavala and Maverick County (Fig. 3), Fry (2015) noted that individual ash beds number 176 in 140 feet of core and well over 300 in 600 feet of core, respectively. In outcrop, ash beds are typically recessive due to the high clay mineral content (Fig. 4). Visual appearance varies slightly between rusty red, white, and purple depending on the amount of iron or manganese leaching. In thin section, ash beds are composed of angular phenocrysts of quartz, K–feldspar, and abundant clay mineral matrix (Fig. 6A). Unweathered ash beds are white/grey in white light and fluoresce bright green under ultraviolet light (Fig. 6B). Some ash beds are partly dolomitized. Although calcite- and dolomite-altered ash beds are not prevalent, nearly all ash beds display alteration of volcanic glass to kaolinite, illite-smectite, and Ca montmorillonite clay mineral species (Table 3).

Ash beds are typically characterized by a sharp basal contact and display a fining upward pattern of phenocrysts observed in thin section (Fig. 6A), likely due in part to differential settling of minerals in the water column. The majority of ash beds appear to have resisted major reworking by bottom current scouring. However, in each of the study areas, a subset of ash beds

**Table 2. A breakdown of which samples underwent U–Pb dating, XRD analysis, oxide XRF, and REE analysis.**

| Sample | Sample Location | U–Pb Dating | XRD | Oxide XRF | REE |
|---|---|---|---|---|---|
| 13–1 | Comstock, TX | X | X | X | X |
| 13–2 | Comstock, TX | | X | X | X |
| 42–1 | Comstock, TX | X | X | X | X |
| 42–2 | Comstock, TX | | X | X | X |
| 42–Top | Comstock, TX | | X | | |
| 51–1 | Comstock, TX | X | X | X | X |
| 51–2 | Comstock, TX | | X | X | X |
| 51–3 | Comstock, TX | | X | X | X |
| 54–1 | Comstock, TX | | X | X | X |
| 54–2 | Comstock, TX | X | X | X | X |
| 54–3 | Comstock, TX | | X | X | X |
| 54–4 | Comstock, TX | X | X | X | X |
| Unit E | Comstock, TX | X | | | |
| Debrite | Comstock, TX | | X | | |
| Del Rio | Comstock, TX | | X | X | X |
| SL–1 | Austin, TX | X | X | X | X |
| SL–2 | Austin, TX | | X | X | X |
| SL–5 | Austin, TX | X | X | X | X |
| SL–6 | Austin, TX | X | X | X | X |
| K1–C1B11 | Karnes County, TX | X | | | |
| K1–C1B2 | Karnes County, TX | X | | X | X |
| K2–C1B18 | Karnes County, TX | X | | X | X |
| A1–C2B11 | Atascosa County, TX | X | | | |
| A1–C1B11 | Atascosa County, TX | X | | | |

were observed to be locally eroded and displaying high levels of reworking. However, few thin ash beds observed in cores C1, K2, and Z1 from the Maverick Basin show reworking and small erosional features (Fry, 2015).

## Mineralogy

Mineralogical analysis was conducted on 18 ash beds collected throughout the stratigraphic column using X-ray diffraction (XRD) by KT Geosciences. Samples were analyzed from surface exposures, but not from the subsurface due to insufficient volumes of material. The whole rock mineralogy of the ash beds is dominated by phyllosilicates, with wide ranging values of quartz, K–feldspar, calcite, and dolomite, along with trace amounts of pyrite, hematite, and gypsum (Table 3). Three ash beds (Del Rio, sample Del Rio; and Boquillas Formation, samples 51–3 and 52–2) with high clay mineral abundances, yielded elevated values of quartz (31–60%) relative to the rest of the dataset. Two of these ash beds (Boquillas Formation, samples 51–3 and 52–2) are located at the base of the Eagle Ford just above the contact with the Buda, while the third ash (sample Del Rio) is from the older Del Rio Formation, underlying the Buda (Fig. 2). Ash beds collected higher in the section all contained reduced quartz demonstrating compositionally more mafic ash beds upsection compared to the base of the Eagle Ford. Calcite diagenesis is more prominent in 12 samples with measurable weight percentages ranging from 0.5–25.8% calcite. While calcite abundance is greatest in two ash beds (samples 51–1 and 13–1) in the lower Eagle Ford, no obvious stratigraphic correlations are apparent and local diagenesis is likely the key factor for the variability observed. Pyrite is present in all samples from the Austin site due to minor weathering, while a lack of pyrite in all West Texas area samples suggests a high degree of weathering.

## Oxide XRF Analysis

Oxide XRF analysis provided helpful data to understand the composition of the magma from which the ash was sourced. A standard total alkaline versus silica plot was constructed and values were plotted against known values for magmatic chemistries (Fig. 7A). Initial values were heavily diluted due to a relatively high percentage of sample lost on ignition (LOI) as a result of water, small amounts of organic matter or liquid hydrocarbons, and sulfur (not measured). Values for LOI range from 10–24%. Values for $SiO_2$, $Na_2O$, and $K_2O$ were recalculated with the subtraction of LOI, with the remaining values representing the whole rock composition. Compositions range from those typical of ultrabasic foidites (38% $SiO_2$) to a highly enriched acidic dacites and rhyolites (79% $SiO_2$). Samples with intermediate values are characteristic of basaltic and andesitic compositions. Using the abundance of quartz as a key indicator, no trends could be determined for the source of ash beds. In both the Comstock outcrops and in the Austin pit (Table 2), acidic and mafic sources were found indicating multiple sources were active during Eagle Ford time. Low values for total alkaline oxides (range of 0.15–2.87%) are observed in all outcrop and shallow subsurface ash beds, while comparing the two ash beds from the subsurface (K1–C1B2 and K2–C1B18), where high values for alkaline oxides (6.32–6.44%) are present.

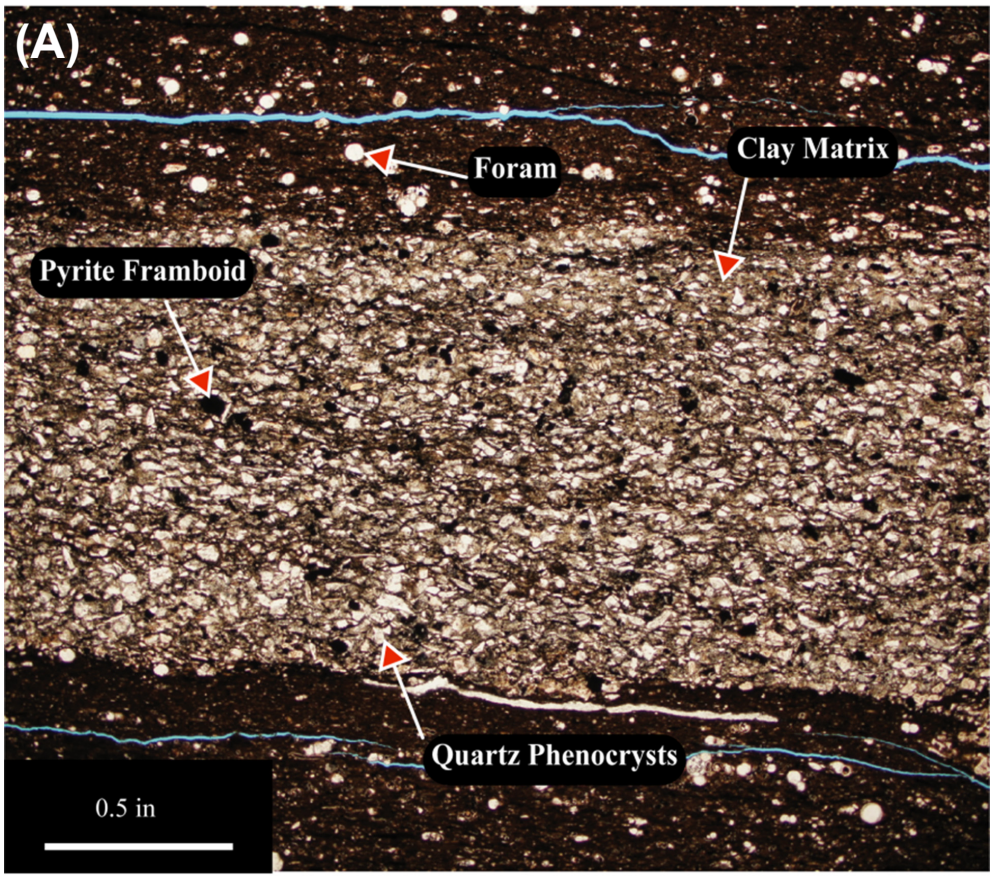


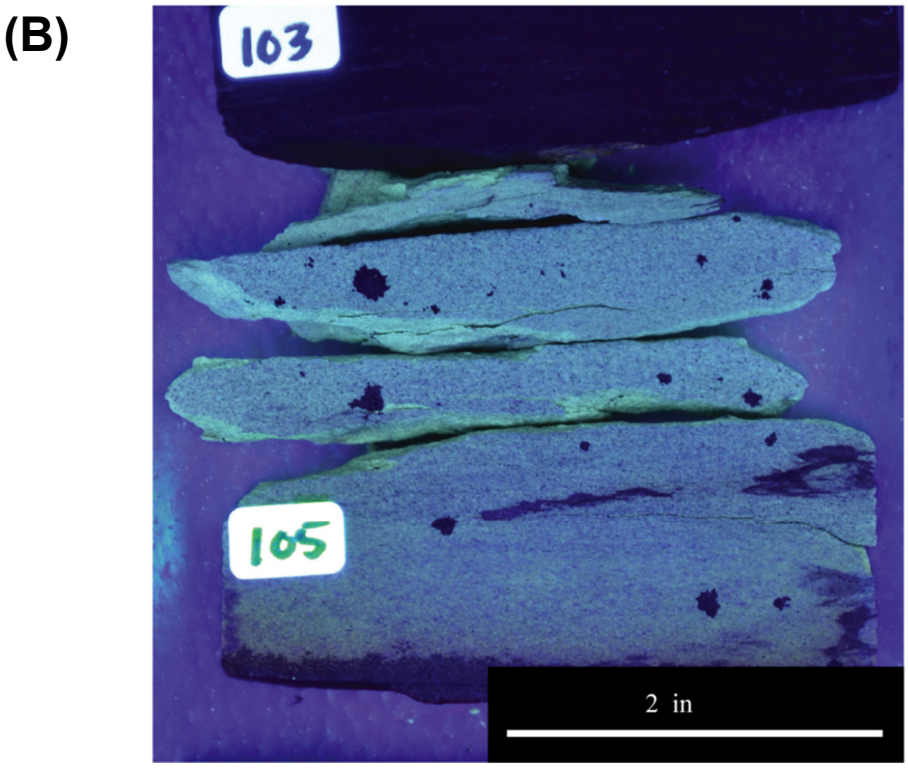


**Figure 6. Photographs showing typical ash bed characteristics. (A) Thin section photomicrograph of a thin ash bed in core Z1. Note the sharp base and the angular phenocrysts that are common indicators of all Eagle Ford ash beds. The mineralogy of the phenocrysts is dominantly quartz, K–feldspar, while the matrix is dominated by montmorillinite and kaolinite clay. (B) Core slab (Z1) photograph of a thick ash bed displaying the yellow-green fluorescence when exposed to long wavelength ultraviolet light. Ash beds from the subsurface fluoresce, while outcrop ash beds that have been exposed to substantial weathering rarely fluoresce.**

**Table 3. Results of the XRD analysis performed on 18 ash bed samples. Ash beds were predominantly composed of clay mineral species, with highly variable amounts of quartz, K–feldspar, and calcite.**

| Sample ID | Del Rio | SL–1 | SL–2 | SL–5 | SL–6 | 54–1 | 54–2 | 54–3 | 54–4 | 42–1 | 42–2 | 13–1 | 13–2 | Debrite | 42–Top | 51–1 | 51–2 | 51–3 |
|---|---|---|---|---|---|---|---|---|---|---|---|---|---|---|---|---|---|---|
| Quartz | 30.7 | 1.6 | 0.9 | 1.1 | 1.4 | 2.8 | 2.7 | 6 | 6.5 | 15.1 | 9.4 | 1.6 | 8.4 | 17.1 | 13.8 | 16.5 | 60.4 | 38.8 |
| K–Feldspar | 0 | 2.9 | 2 | 2.9 | 3.3 | 0 | 0 | 0 | 2.7 | 5.6 | 5.3 | 0 | 0 | 0 | 4 | 0 | 0 | 0 |
| Calcite | 15.2 | 0 | 0 | 0 | 0 | 2.4 | 2.8 | 1.9 | 1.7 | 1.9 | 2.7 | 2.5 | 12.3 | 19.6 | 2.5 | 25.8 | 0.5 | 0 |
| Dolomite | 0 | 0 | 0 | 0 | 0 | 0 | 0 | 0 | 0 | 0 | 0 | 0 | 0 | 57.4 | 0.7 | 0 | 0 | 0 |
| Pyrite | 0.6 | 26.2 | 1.1 | 1 | 0.9 | 0 | 0 | 0 | 0.8 | 0 | 0 | 0 | 0 | 0 | 0 | 0 | 0.4 | 0 |
| Marcasite | 0 | 0 | 0 | 0 | 0.3 | 0 | 0 | 0 | 0 | 0 | 0 | 0 | 0 | 0 | 0 | 0 | 0 | 0 |
| Hematite | 0 | 0 | 0 | 0 | 0 | 0.2 | 0 | 0 | 0 | 4.5 | 3.6 | 0 | 1.2 | 0 | 0.9 | 1.4 | 0 | 0.8 |
| Gypsum | 0 | 3.2 | 0.4 | 0.3 | 0.8 | 0 | 0 | 0 | 0 | 0 | 2.5 | 0 | 0 | 0 | 29 | 0 | 0 | 0 |
| Halite | 0 | 0 | 0 | 0 | 0 | 0 | 0 | 0 | 0 | 0 | 0 | 0 | 0 | 0 | 0 | 2.6 | 0 | 0 |
| Ca Montmorillonite | 0 | 0 | 74.2 | 77.2 | 67.9 | 0 | 0 | 0 | 0 | 0 | 0 | 0 | 0 | 0 | 0 | 0 | 0 | 0 |
| R0 M–L I/S (90%S) | 4.3 | 14.2 | 0 | 0 | 0 | 0 | 0 | 0 | 0 | 0 | 0 | 0 | 0 | 0 | 0 | 0 | 4.3 | 0 |
| R1 M–L I/S (30%S) | 7.7 | 0 | 0 | 0 | 0 | 0 | 0 | 3.1 | 0 | 10.8 | 19.7 | 0 | 0 | 0.5 | 10.7 | 2.6 | 8.4 | 0 |
| Illite & Mica | 10.3 | 5.9 | 1.8 | 0 | 1.4 | 0 | 0 | 0 | 2 | 3.1 | 2.7 | 0 | 0 | 0.8 | 3.7 | 4.3 | 7 | 1.5 |
| Kaolinite | 31.2 | 46 | 19.6 | 17.5 | 24 | 94.6 | 94.5 | 89 | 86.3 | 59 | 54.1 | 95.9 | 78.1 | 4.6 | 34.7 | 46.8 | 19 | 58.9 |
| **Total** | **100** | **100** | **100** | **100** | **100** | **100** | **100** | **100** | **100** | **100** | **100** | **100** | **100** | **100** | **100** | **100** | **100** | **100** |

## Rare Earth Element Analysis

Chondrite normalized rare earth element (REE) plots (Fig. 7B) demonstrate enrichment in light REE with values ranging from 17 to 300 for La. Eu anomalies as represented by $Eu/(Sm*Gd)^{0.5}$, are significant in all three study locations. In the Comstock area, values for Eu range in value from 0.35 to 0.96. Negative Eu anomalies exist for all samples from Comstock with the exception of 42–1 and 42–2. These two samples show no positive or negative anomalies and indicate a different source magma composition. With values from 0.32 to 0.41, three Austin area ash beds (Bouldin Member, samples SL–1, SL–5, and SL–6) show no negligible anomalies. However, the upper ash bed from the Austin study site (Bosque Formation, sample SL–2) has a significant positive anomaly with a value of 1.07. The two subsurface ash beds (Austin Chalk Formation, samples K1–C1B2, K2–C1B18) yield values of 0.29 and 0.39 indicating strong negative Eu anomalies. The lack of Eu anomalies for two ash beds in the upper Eagle Ford (Boquillas Formation, samples 42–1 and 42–2) indicate a more arc related source, while the negative Eu anomalies seen in other samples indicate a more basaltic source. The heavy rare earth elements (HREE) are highly fractionated compared to middle rare earth elements (MREE), as documented by sample Sm/Yb ratios. Values for ash beds from Comstock area outcrops range from 1.58 to 6.93, 1.48 to 5.71 for Austin pit samples, and 3.26 to 4.05 for subsurface samples. The light rare earth elements (LREE) enrichment with the depletion of HREE of many samples is similar to what was seen by Griffin et al. (2008) and what has been described as partial melting of garnet peridodite. Three ash beds across all study areas (South Bosque, Boquillas, and Eagle Ford formations, samples SL–2, 42–2, and K1–C1B2, respectively) show limited enrichment in LREE, with little depletion of the HREE, a pattern often observed in basaltic rocks.

## U–Pb Geochronology

**Eagle Ford Equivalent Boquillas Formation Outcrops near Comstock West Texas:** Six ash beds were collected from outcrops near Comstock, Texas (Fig. 3). Results of the U–Pb LA–ICP–MS dating are shown relative to a composite stratigraphic section in Figure 8. At outcrop 51 (Table 4), a thin ash bed is present (sample 51–1) at the basal contact of the Boquillas and Buda. A coherent group of 42 crystals yielded a weighted mean age of 96.8 +1.2/-0.7 Ma (Table 4).

The next prominent ash bed (sample 13–1) is located 66 feet above the base of the Boquillas and 32 feet below the upper Boquillas and lower Boquillas contact, totaling a coherent group of 28 crystals that yielded a weighted mean age of 96.4 +1.4/-1.0 Ma (Table 4). This ash bed represented the most complex zircon population of the study. High levels of common Pb observed in 20 single crystals yielded discordant results and, thus, were unacceptable for age calculations. Many grain results are still discordant because of common Pb, but are still used in the calculations because discordance values are less than 10%. This has the impact of slightly increasing the relative calculated age of the sample.

Two samples were dated at outcrop 54. The lowest ash bed (sample 54–4) lies 8 feet above sample 13–1. A coherent group of 17 crystals yielded a weighted mean age of 94.10 +1.0/-1.40 Ma. Common Pb and inheritance were a contributing factor to the high mean square weighted deviation (MSWD). A coherent group of 48 crystals from a second sample (sample 54–4) taken 88 feet above the Buda contact yielded a weighted mean age of 93.45 +0.75/-0.65 Ma.

A thick ash bed (sample 42–1) is located roughly 8 feet above the thick calcarenite bed marking the unit B–C contact. A coherent group of 21 crystals yielded a weighted mean age of 92.4 +0.2/-1.2 Ma. This ash bed (sample 42–1) contained low abundances of zircon, although at 8 inches thick, it was the second thickest ash bed in the collection suite.

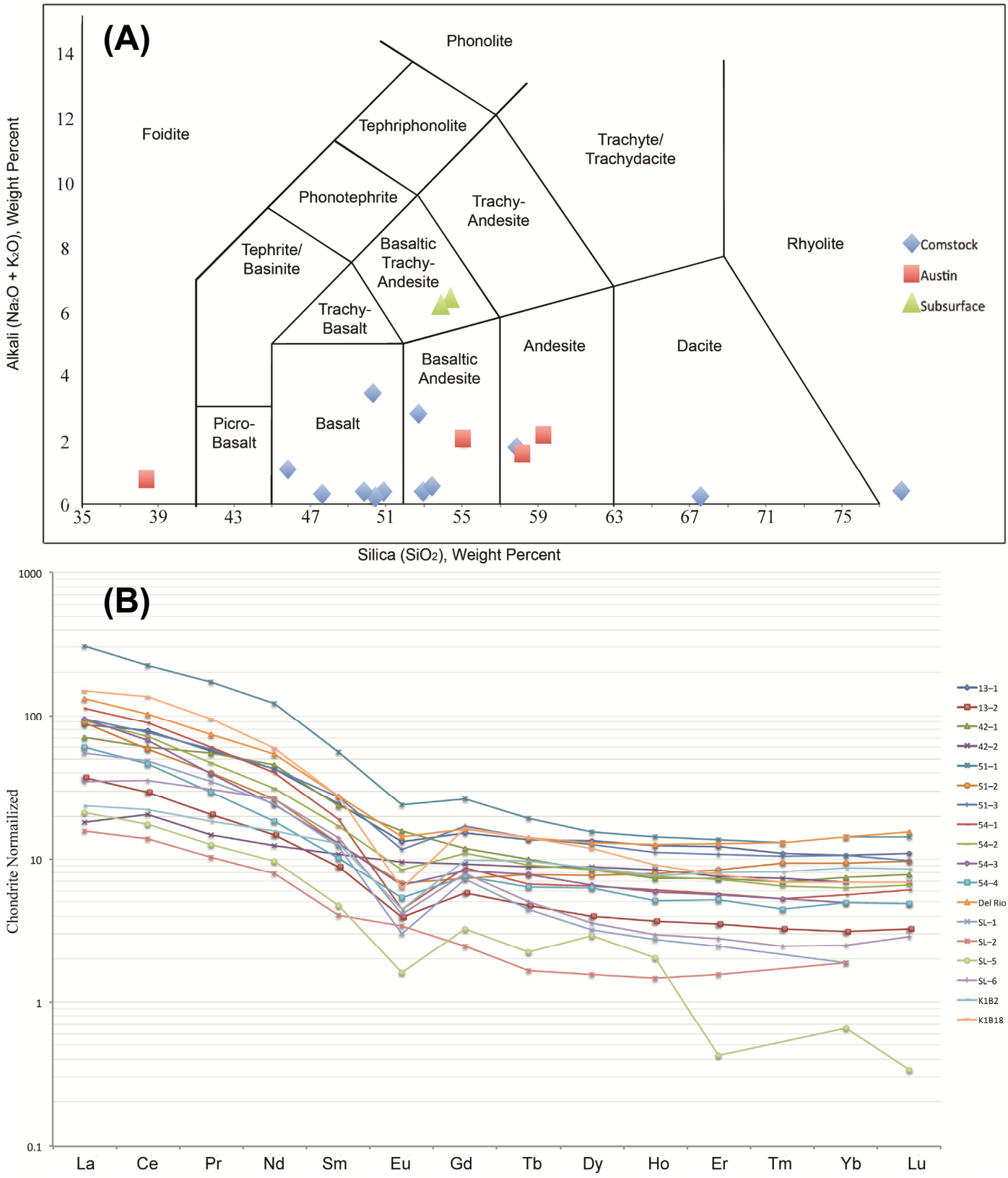


**Figure 7. Ash bed geochemistry used to help differentiate whether single or multiple eruptive sources were responsible for the numerous ash beds found in the Eagle Ford and equivalent Boquillas. (A) Total alkali versus silica plot from ashes of all three study locations. A wide range of total silica is observed with samples ranging from ultrabasic to acidic. Low values of total alkali in all outcrop samples compared with the subsurface samples may indicate potential leaching during the weathering process. (B) Rare earth element (REE) plot versus chondrite normalized values from McDonough and Sun (1995). Samples are generally enriched in heavy REE and depleted in light REE, however two samples show no significant enrichment of heavy REE compared to light REE. This variation suggests both arc and basaltic volcanism. Negative Eu anomalies exist for all samples except S–2, 42–1, 42–2. Sample SL–2 data indicates a slight positive Eu anomaly. The variability seen in the REE plots indicate multiple volcanic sources.**

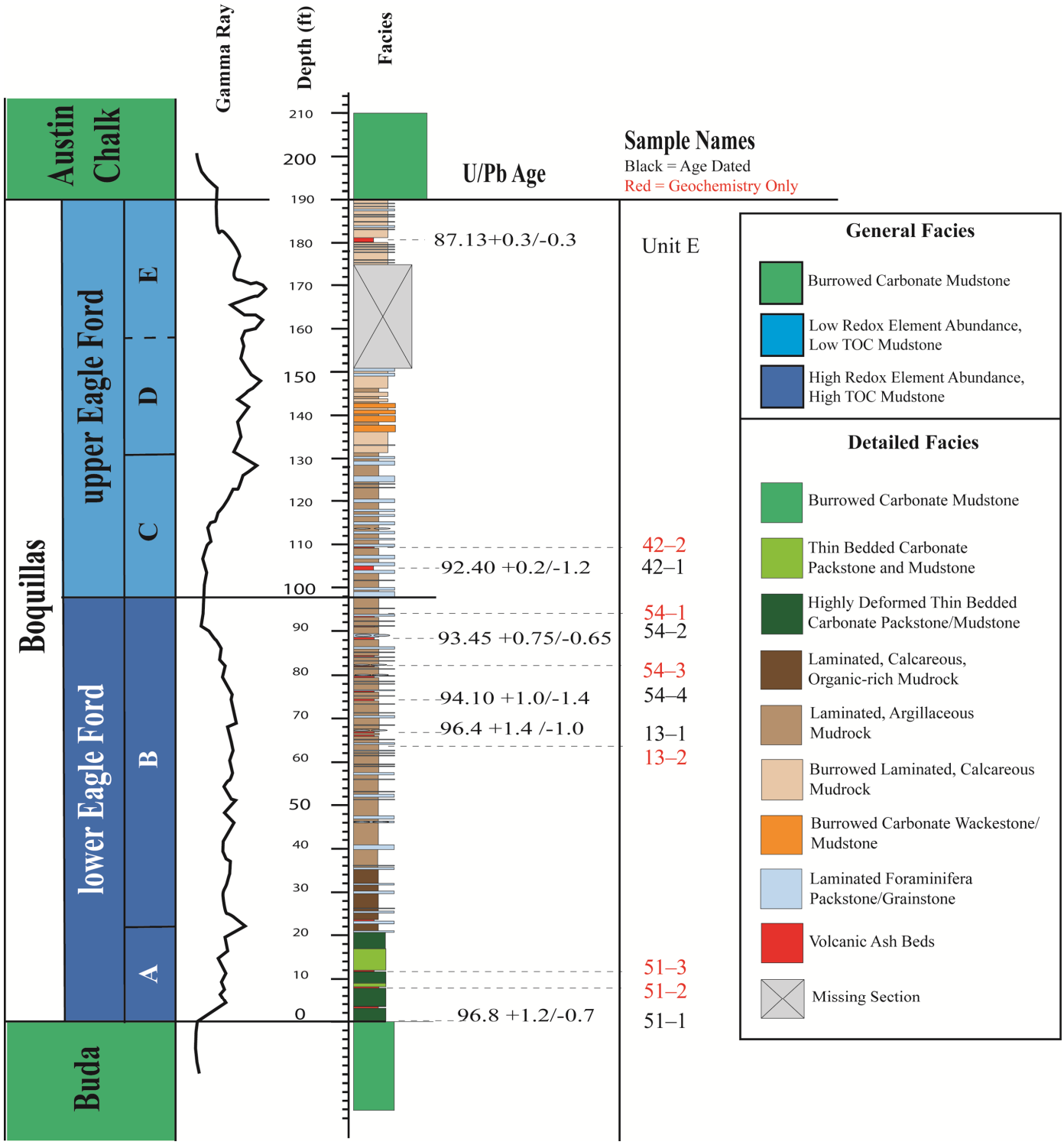


**Figure 8. Composite stratigraphic section of the Boquillas (Eagle Ford equivalent) Formation in the Comstock outcrop study area (Fig. 3) showing sample locations and ash bed age dates. Detailed facies description completed at roadside outcrops 51, 13, 42, and unit E (Table 4).**

Samples were also taken from a 9 inch thick ash bed 9 feet below the Austin Chalk contact (sample unit E) just east of Lozier Canyon (Fig. 3). A coherent group of 84 crystals yielded a weighted mean age of 87.13 ± 0.3 Ma. TuffZirc defined a coherent group that included a large portion of grains with obvious Pb loss. As a consequence, a manual weighted mean age was calculated by omitting zircons with clear Pb loss.

### Subsurface Core in South Texas

Samples were taken from subsurface cores A1, K1, and K2 located in Atascosa and Karnes counties (Fig. 3). The lowest ash bed sample (A1–C2B11) was taken at 7779 feet core depth, roughly 11 feet above the Buda–Eagle Ford contact (Fig. 9). A coherent group of 40 crystals yielded a weighted mean age of 94.66 ± 0.36 Ma (Table 4). A second ash bed sample (A1–

**Table 4. Ash sample locations for each sample collected. Samples locations collected in the subsurface are confidential and thus only county is provided. Calculated $^{206}Pb/^{238}U$ ages are plotted along with their associated uncertainty, $^{207}Pb/^{206}Pb$ vs. $^{206}Pb/^{238}U$ age and uncertainty, mean square weighted deviation (MSWD), and coherent group.**

| Sample Name | Location | Latitude | Longitude | Weighted Mean Average (Ma) | Uncertainty (Ma) | $^{207}Pb/^{206}Pb$ vs. $^{206}Pb/^{238}U$ Age (Ma) | Uncertainty (Ma) | MSWD | Zircons Analyzed | Coherent Group | Core Depth |
|---|---|---|---|---|---|---|---|---|---|---|---|
| 51–1 | Comstock, TX | 29°49'3.20"N | 101°35'57.66"W | 96.8 | +1.2 / -0.7 | 94.21 | ±0.82 | 4.2 | 57 | 42 | – |
| 13–1 | Comstock, TX | 29°42'36.55"N | 101°14'21.40" | 96.4 | +1.4 / -1.0 | 93.61 | ±0.93 | 5.5 | 58 | 28 | – |
| 54–4 | Comstock, TX | 29°49'27.84"N | 101°37'0.54"W | 94.1 | +1.0 / -1.4 | 94.8 | ±1.0 | 11 | 37 | 17 | – |
| 54–2 | Comstock, TX | 29°49'27.84"N | 101°37'0.54"W | 93.45 | +0.75 / -0.65 | 92.16 | ±0.69 | 4.6 | 78 | 48 | – |
| 42–1 | Comstock, TX | 29°48'33.90"N | 101°30'29.02"W | 92.4 | +0.2 / -1.2 | 91.2 | ±0.85 | 7.1 | 27 | 21 | – |
| Unit E | Comstock, TX | 29°54'9.90"N | 101°46'50.26"W | 87.13 | ±0.3 | 86.76 | ±0.52 | 16 | 164 | 84 | – |
| A1–C2B11 | Atascosa Co., TX | – | – | 94.66 | ±0.55 | 94.17 | ±0.77 | 8.6 | 75 | 40 | 7779 |
| A1–C1B11 | Atascosa Co., TX | – | – | 91.95 | ±0.37 | 90.14 | ±0.77 | 15 | 59 | 42 | 7690 |
| K2–C1B18 | Karnes Co., TX | – | – | 89.5 | +0.4 / -0.8 | 87.29 | ±0.79 | 13 | 65 | 42 | 12,141 |
| K1–C1B11 | Karnes Co., TX | – | – | 93.7 | ±0.4 | 92.78 | ±0.45 | 4.5 | 85 | 68 | 11,778 |
| K1–C1B2 | Karnes Co., TX | – | – | 89.75 | +0.35 / -0.45 | 88.16 | ±0.44 | 5 | 58 | 54 | 11,747 |
| SL–5 | Austin, TX | 30°15'20.34"N | 97°45'44.08"W | 96.3 | +1.1 / -1.0 | 95.41 | ±0.65 | 3 | 56 | 35 | – |
| SL–6 | Austin, TX | 30°15'20.34"N | 97°45'44.08"W | 93.2 | +0.4 / -0.3 | 92.92 | ±0.72 | 16 | 106 | 61 | – |
| SL–1 | Austin, TX | 30°15'20.34"N | 97°45'44.08"W | 91.6 | +0.6 / -0.4 | 91.89 | ± 0.94 | 11.7 | 60 | 39 | – |

C1B11) was collected at a core depth of 7690 feet, roughly 12 feet below the Austin Chalk contact. A coherent group of 42 crystals from this sample yielded a weighted mean age of 91.95 ± 0.55 Ma.

Cored well K2 was drilled approximately 25 miles from the A1 core (Figs. 3 and 8). The K2 core contains 175 feet of Eagle Ford facies, including the contact with the Austin Chalk, but missing the basal contact with the Buda by 10 feet or less. A single sample (K2–C1B18) was taken in the Austin Chalk facies, 18 feet above the Eagle Ford–Austin Chalk contact at a core depth of 12,141 feet. A coherent group of 42 crystals from this sample yielded a weighted mean age of 89.50 +0.4/-0.8 Ma.

Cored well K1 is located approximately 4 miles east of K2 (Figs. 3 and 8). K1 contains 190 feet of Eagle Ford facies, including the contacts with the Buda and Austin Chalk. The lowest ash bed sample (K1–C1B11) was collected at a core depth of 11,778 feet in the upper Eagle Ford (Fig. 9). A coherent group of 68 crystals yielded a weighted mean age of 93.70 ± 0.4 Ma. This sample has little in the way of Pb loss or common Pb. However, it appears to have a large amount of inheritance in all crystals tested leading to an older than eruptive age. A second ash bed sample (K1–C1B2) was taken from a core depth of 11,747 feet within the Austin Chalk. A coherent group of 54 crystals from this sample yielded a weighted mean age of 89.75 +0.35/-0.45 Ma.

### Shallow Subsurface Pit Site in Austin, Texas

Four ash beds were collected from a construction pit in Austin, Texas (Figs. 3 and 10). In this area the Eagle Ford is subdivided into four units: the basal Pepper Shale, the Waller Member, the Bouldin Member, and the South Bosque Formation, all representing the Eagle Ford (Fig. 2) (Fairbanks, 2012). The Bouldin–South Bosque contact represents the transition from lower to upper Eagle Ford. In the construction pit, only the South Bosque Formation and the Bouldin Member are present, along with the contact with the Austin Chalk. Sample SL–5 was collected from the base of the Bouldin member. A coherent group of 35 crystals yielded a weighted mean age of 96.3 +1.1/-1.0 Ma. A 6 inch ash bed (sample SL–6) was collected 8 feet above SL–5, at the top of the Bouldin Member. A coherent group of 61 crystals yielded a weighted mean age of 93.20 +0.4/-0.3 Ma. This sample is a very high-resolution U–Pb age with little issues from inheritance, common Pb, and Pb loss. Sample SL–1 was collected in the South Bosque Formation, 6 feet below the Eagle Ford–Austin Chalk contact. A coherent group of 39 crystals yielded a weighted mean age of 91.60 +0.6/-0.4 Ma.

## DISCUSSION

## Active Volcanism in North America during the Cenomanian through Coniacian

### Eagle Ford/Boquillas Ash Beds

The volcanic ash deposits found within the Eagle Ford have been a poorly studied facies until recently. Their presence has been documented in recent publications (e.g., Hazzard, 1959; Surles, 1986; Donovan et al., 2012; Eldrett et al., 2014, 2015a, 2015b), but no attempt has been made to identify their composition or source(s). Numerous studies have focused on the bentonite beds north of the Eagle Ford in the Western Interior Seaway, with most attention given to ashes near the C–T Global Boundary Stratotype Section Point (GSSP) in Pueblo, Colorado (Elder, 1988; Obradovich, 1993; Meyers et al., 2012; Ma et al., 2014; Sageman et al., 2014). While some of the ash beds in the Western Interior Seaway may correlate to some Eagle Ford ash beds (Fig. 1), and may be partially sourced by the same volcanoes, no such correlations have been proven. To attain a better under-

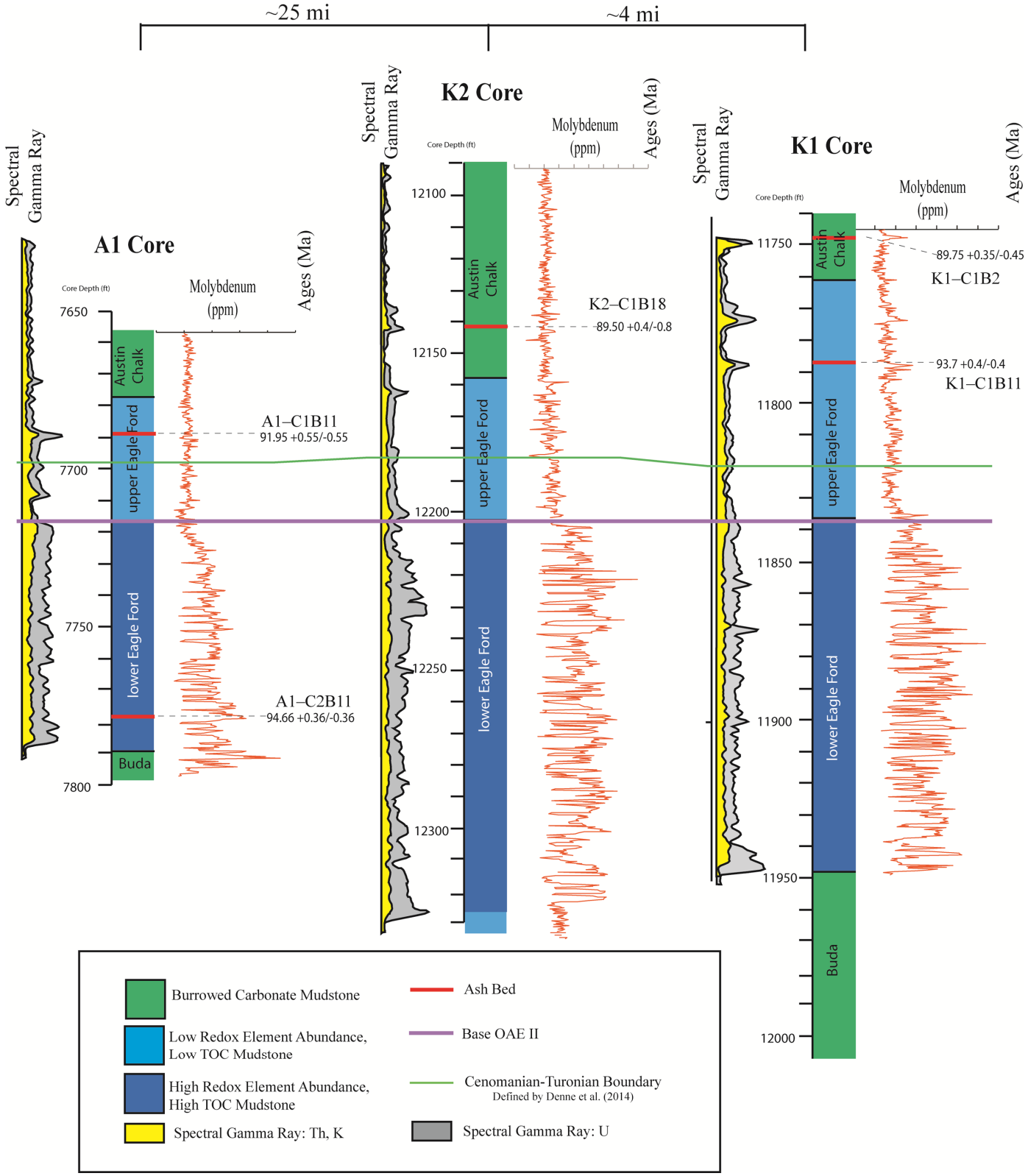


**Figure 9. Cross section showing sample locations and U–Pb ash bed age dates for subsurface cores. Upper and lower Eagle Ford subdivisions based on upward change from anoxic to oxic conditions utilizing uranium and molybdenum as proxies for oxygen levels and organic matter abundance. Note depths are core depths.**

standing of the potential source areas for the Eagle Ford ash beds, it is vital to look at all documented volcanic activity from Albian to Santonian in North America.

To accurately determine the volcanic sources of the Eagle Ford ash beds, an understanding is needed of geochemical properties of the ash beds, direction of dominant paleowinds, and

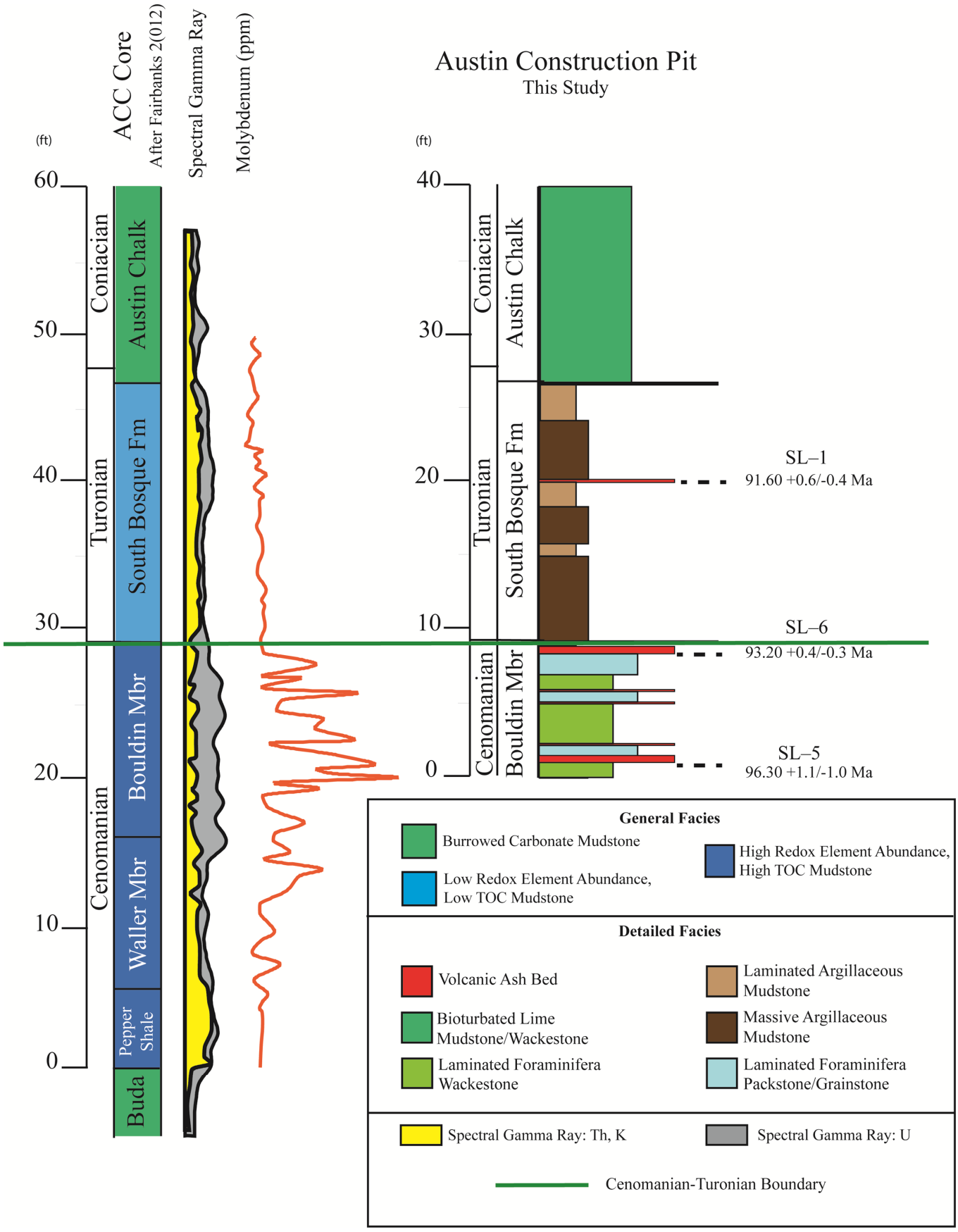


**Figure 10. Stratigraphic columns showing sample locations and U–Pb age dates for dated ash beds from construction pit locality and correlations to nearby subsurface ACC core in Austin, Texas (Fig. 3). Placement of Cenomainian/Turonian boundary in the ACC core from Corbett and Watkins (2103). General facies breakdown for the ACC core from Fairbanks (2012) and Fairbanks et al. (2016). The lowermost Eagle Ford was not exposed at this location.**

insight into distances ash can travel while accumulating in thicknesses observed in the Eagle Ford. The chemical makeup of the Eagle Ford ash beds is difficult to precisely define due to the intense alteration that these water laid ashes have undergone. This makes standard geochemical procedures less effective and requires a more in-depth analysis. Additionally, the direction of paleowinds plays a large role in ash trajectory and distance from the source. South Texas during the Cenomanian through Coniacian was located at ~30° north latitude (Roberts and Kirschbaum, 1995; Blakey, 2012) (Fig. 1). It has been hypothesized that, during the super greenhouse of the mid-Cretaceous, the westerly trade winds that are typically associated with higher latitudes were present at 30° north due to a shrinking of the global Hadley cells (Hasegawa et al., 2012). In addition to paleowind direction, understanding the distances that ashes can travel is equally important. Ash is dispersed and deposited over great distances and thins away from the source according to the exponential thinning law (Pyle, 1989). Studies have indicated that airborne ash can travel around the globe, but thick ash accumulations pre-compaction of more than 8 inches can have traveled no more than 250 miles from their source (Slaughter and Hamil, 1970; Elder, 1988; Sparks et al., 1992; Mastin et al., 2009; Gonzalez-Mellado and de la Cruz-Reyna, 2010). This greatly limits the possible sources for the thickest Eagle Ford ash beds to a much more local area (Fig. 1).

The Late Cretaceous was a period of frequent volcanism globally with numerous large igneous provinces (LIPs) active during the Cenomanian-Turonian and additional widespread volcanism occurring more locally in North America (Fig. 1) (Stott, 1963; Gill and Coban, 1973; Armstrong et al., 1977; Toth, 1985; Mahoney et al., 1993; Storey et al., 1995; Tejada et al., 1996; Sinton and Duncan, 1997; Sinton et al., 1998; Ramana et al., 2001; Alexandre et al., 2012). The following are the most plausible potential sources for the Eagle Ford ash beds. Other less likely, but possible sources of volcanism during Eagle Ford time, are given in Figure 1.

### South-Central Arkansas

A small grouping of igneous activity is located in South-Central Arkansas in close proximity to the Gulf Coast. Ross et al. (1929) first recognized this Cretaceous volcanism and concluded that numerous volcanic centers existed around Nashville, Murfreesboro, Prairie Creek, and Lockesburg, Arkansas, which are compositionally ultrabasic (peridotitic and lamproite), with possible trachytic vents (Hunter and Davies, 1979; Dunn, 2002). K–Ar dating of the Prairie Creek lamproites indicates Late Cretaceous ages ranging from 106–97 Ma (Zartman, 1977).

### Balcones Igneous Province

In Central and Southeast Texas, the Balcones Igneous Province was a center of sizable volcanic activity in the Late Cretaceous. The Balcones Igneous Province manifests as a swarm of numerous small intrusion and eruptive centers that are concentrated mainly in the South Texas counties of Uvalde, Kinney, and Medina, but extends up through Travis County with the well-studied Pilot Knob (Ewing and Caren, 1982). A magmatic study of the area indicated upwards of 200 individual intrusions in the Uvalde area, with only 30 exposures on the surface (Smith et al., 2002). Geochemistry of the exposed intrusions has indicated compositions of a monogenic alkaline volcanic system (Griffin et al., 2010). Of the 30 exposures, many have been dated radiometrically using K–Ar, Ar–Ar, and U–Pb dating. Initial K–Ar age dating done by Baldwin and Adams (1971) yielded an age range of 86–63 Ma for the exposed intrusions in Uvalde County, while higher precision Ar–Ar and U–Pb geochronology conducted by Miggins et al. (2004) and Griffin et al. (2010) yielded age ranges of 82–72 Ma and 84–76 Ma, respectively. Barker (1996) indicated that there are intrusions that are significantly older than radiometric ages, pointing out a stratigraphic relationship between volcaniclastic mudflows interbedded with the older Del Rio Formation (Fig. 2). While modern high-precision geochronology has helped refine the age and duration of the Balcones Igneous Province, the occurrence of more than 200 subsurface intrusions suggests that additional work needs to be undertaken in order to more comprehensively understand the true duration of the Balcones Igneous Province.

### Western Mexico

Widespread volcanic activity has been documented west of Texas in Mexico during the Late Cretaceous (Elder, 1988; Silver et al., 1993; McDowell et al., 2001; Centeno-Garcia et al., 2008). This volcanism is focused in two separate locations. The northern activity is located in the Sonora region and has been dated through various radioisotopic studies. While it is well understood that the majority of the arc volcanism occurred along the western coast of Mexico, volcanism was also active in eastern Sonora around 90 Ma (McDowell et al., 2001). To the south in the vicinity of Zihuatanejo, more Cenomanian-Turonian volcanism has been recorded. Arc magmatism along much of the western coast of Mexico has been proposed to have occurred at its peak from Late Jurassic through the Early Cretaceous with the volcanism in the Zihuatanejo terranes continuing to the Cenomanian time (Centeno-Garcia et al., 2008).

## Source of Eagle Ford/Boquillas Ash Beds

The low silica chemical composition of the thick ash beds in the Austin pit locality (SL–6 upper Eagle Ford) and in subsurface core K2 (K2–C1B18 basal Austin Chalk) (Figs. 8 and 9), indicates an intermediate composition with silica values plotting in the basaltic andesite area (Fig. 7A). All thin ash beds analyzed display a wide range of silica content from 38–79% silica. The high silica ash bed samples also plot with high values of HREE and depleted LREE indicating a volcanic arc source likely from the Sonora area of western Mexico. Values for alkali oxides in the surface ash bed samples from the Comstock and Austin areas yield lower quality results due to the high alteration in many of the samples. However, the two subsurface ash beds (samples K2–C1B18 and K1–C1B2) display elevated values of alkali oxides, indicating that the least altered ash beds contain elevated amount of K and Na and that weathered samples likely contained more original K and Na. A misinterpretation of K and Na values without considering the effects of weathering would potentially lead to the misidentification of the magma source.

In analyzing the compositional variability of the ash beds, it is concluded that multiple sources existed for the Eagle Ford ash beds. Additionally, examining the physical thickness of the ash beds helped further refine potential sources. All study locations contained ash beds greater than 8 inches thick with outcrop beds displaying no observable thinning eliminating any clues about direction of sources. However, these thick ash beds (8 inches and greater) strongly suggest the occurrence of a proximal local/regional volcanic source due to maximum transport distances of approximately 250 miles (Slaughter and Hamil, 1970; Elder, 1988; Sparks et al., 1992; Mastin et al., 2009; Gonzalez-Mellado and de la Cruz-Reyna, 2010). Arc volcanism in northern Mexico and southern Arizona are the most likely the sources for the more silica-rich ash beds found in the Comstock area near the basal contact with the Buda. The two thick Comstock area ash beds in the upper Eagle Ford (42–1 and unit E) (Fig. 8), however, display more intermediate to ultrabasic chemistries. Additionally, these two ash beds contain Neoproterozoic xenocrysts of ages similar to the 550–780 Ma ages recorded in Balcones Igneous Province radioisotopic studies (Griffin 2010, Gleason et al., 2007). This xenocrystic population is thought to be sourced from the Ouachita Orogenic Belt that underlies much of Central and South Texas,

indicating that zircons found in both the Balcones Igneous Province and Eagle Ford ash beds may have the same xenocrystic core and, thus, same source (Griffin, 2010; Gleason et al., 2007). Volcanism in Arkansas and to the north-northwest, into the Western Interior Seaway, may be the source of some of the occasional thin ash beds within the Eagle Ford, but the prevailing paleowind direction was not conducive for prolonged periods of ash deposition from those source areas (Roberts and Kirschbaum 1995; Hasegawa et al., 2012).

## Comparison of West Texas Geochronology with Eldrett et al. (2015)

To date, most research on the Eagle Ford has focused on sedimentology, regional framework through log correlations, pore sizes and distribution, and geochemistry (Donovan and Staerker, 2010; Donovan et al., 2012; Denne et al., 2014; Fairbanks et al., 2016; Frebourg et al., 2016). Papers by Eldrett et al. (2014, 2015a, 2015b), provide the only previous reports of radiometric age dates for Eagle Ford ash beds. While radiometric geochronology is not the primary focus of that study, and the data were restricted to a single core located in Kinney County between the outcrop and subsurface areas sampled for this study (Fig. 3), their work is a significant contribution to our understanding of timing and duration of events during Eagle Ford deposition.

The age obtained from the most basal Eagle Ford ash bed in the Comstock area (Boquillas Formation, sample 51–1) is 96.8 +1.2/-0.7 Ma (Fig. 8). This age is consistent with what Eldrett et al. (2014, 2015a) reported using an ID–TIMS age of 97.6 ± 0.062 Ma proximal to the base of the Eagle Ford. Based on biostratigraphic data reported by Donovan et al (2012), the C–T boundary in the West Texas outcrops is bracketed by this paper's ash bed dates from the middle Boquillas (samples 54–4, 54–2, and 42–1). Ages date the boundary at about 93.45 ± 0.7 Ma. The C–T boundary, as determined by Eldrett et al. (2014, 2015a), is bracketed by two ashes dated at 94.33 ± 0.15 Ma and 93.66 ± 0.037 Ma. This age range is consistent with the accepted age of 93.9 Ma for the C–T boundary previously reported (Meyers et al., 2012; Gradstein et al., 2012). Thus, results from the current study and from Eldrett et al. (2015a) are in close agreement with previous ages reported for the C–T boundary.

The thick ash bed (Boquillas Fm, sample unit E) (Fig. 8) at the top of the upper Eagle Ford near the contact with the Austin Chalk is age dated at 87.13 ± 0.3 Ma. This ash bed is a very thick bed at the top of the Eagle Ford at a similar stratigraphic position to the ash dated by Eldrett et al. (2015a). Eldrett et al. (2014, 2015a) age-dated an ash bed in a similar stratigraphic position from a Kinney County core (~75 miles from Comstock outcrops) 20 feet below the contact with the Austin Chalk at 90.77 ± 0.039 Ma. Although these two ash beds appear similar in thickness and stratigraphic position, the age difference between the two studies results are more than 4.5 million years. While the spread of this study's geochronological results from this ash bed (sample Unit E) have a large MSWD of 16, a total of 164 single crystals were analyzed and of those, only 21 zircons yielded single crystal ages around 91 Ma. Observations in the C1 and Z1 cores (Fig. 3) reveal no ash beds matching the thickness and the stratigraphic position of this ash bed indicating that these ash deposits are almost certainly not correlative. This variation in age indicates that the top of the Eagle Ford varies substantially due to lateral facies changes, erosion, or both. The differences in age dates from large, superficially similar, ash beds reliably reinforce the fact that the Eagle Ford–Austin Chalk boundary is only lithologic and not a chronologic boundary.

Age dates obtained in this study are closely comparable with those measured by Eldrett et al. (2015a). Lithostratigraphic correlations from the Eldrett et al. (2014, 2015a) core to the Comstock area are not entirely reliable as evidenced by two stratigraphically similar ash beds yielding much different ages. This variation and duration of Eagle Ford facies, especially in the upper Eagle Ford is likely due to differing local depositional patterns. Thus reliable ash bed to ash bed correlations cannot be established between these two study areas, and this inability to correlate is consistent with the documented large-scale variability in duration of Eagle Ford strata are observed across the western extent of the formation.

## Comparison of Geochronology with Biostratigraphy

Several papers have been published on the biostratigraphy of the Eagle Ford succession (e.g., Pessagno, 1969; Jiang 1989; Lundquist, 2000; Donovan and Staerker, 2010; Corbett and Watkins, 2013; Denne et al., 2014). This wealth of biostratigraphy allows for important integration of the new U–Pb geochronology presented in the current study to help constrain relative ages derived from faunal biozones determined by Donovan and Staerker (2010) in Lozier Canyon (Fig. 3), Denne et al. (2014) in the subsurface, and Corbett and Watkins (2013) in Austin, Texas.

### Austin Pit Section Comparisons

Corbett and Watkins' (2013) biostratigraphic work of calcareous nannofossils on the ACC #1 core (Fig. 10) provides a significant opportunity to compare biostratigraphy with our U–Pb age dating. At the Austin pit site, the Bouldin Member and the South Bosque Formation were exposed (Figs. 2 and 9). At the base of the Bouldin Member in the ACC core, Corbett and Watkins (2013) defined the strata as middle upper Cenomanian. This is the same stratigraphic interval as our most basal ash (Bouldin Member, sample SL–5) from the Austin pit locality, which was dated at 96.3 +1.1/-1.0 Ma, indicating strata of lower middle Cenomanian. The C–T boundary was defined by Corbett and Watkins (2013) to be at the contact between the Bouldin Member and the South Bosque (Fig. 10). A thick ash bed (Bouldin Member, sample SL–6) was collected from the uppermost Bouldin Member and yielded an age of 93.20 +0.4/-0.3 Ma (Fig. 11). This age is very close to the accepted C–T boundary age, 93.9 Ma, given by Gradstein et al. (2012). No significant biostratigraphic boundary was defined at the position of the uppermost sampled ash bed (South Bosque Formation, sample SL–1), which was dated at 91.60 +0.6/-0.4 Ma. However, the early Turonian age designated for the South Bosque Formation by Corbett and Watkins (2013) aligns with our U–Pb age, indicating an Eagle Ford deposition period that terminated prior to the Turonian-Coniacian boundary.

The U–Pb ages from this study are largely consistent with the nannofossil biozones recognized by Corbett and Watkins (2013) throughout the section. The lowermost ash bed sampled at this site (Bouldin Member, sample SL–5) gave an age of 96.3 +1.1/-1.0 Ma, indicating that strata are likely a little older than the biostratigraphic data suggest. Conversely the age could be slightly older due to complex population of zircons, and thus using an age on the younger end of the uncertainty may pose as a better fit. If the age is accurate as stated, then the underlying Waller Member and Pepper Shale are older than proposed.

### Comstock Area Outcrop Comparisons

Donovan and Staerker (2010) conducted their biostratigraphic analysis in Lozier Canyon (Fig. 3) on units B–E. Two samples collected by Donovan and Staerker (2010) in unit B indicate late Cenomanian age, with a third upper most sample marking the latest of Cenomanian age (Donovan and Staerker, 2010). Exact depths for samples are not given or marked on the complete stratigraphic column, making precise integration with the samples of the present study difficult. Two ash beds (Boquillas Formation, samples 54–4 and 54–2) (Fig. 11) analyzed in the current study

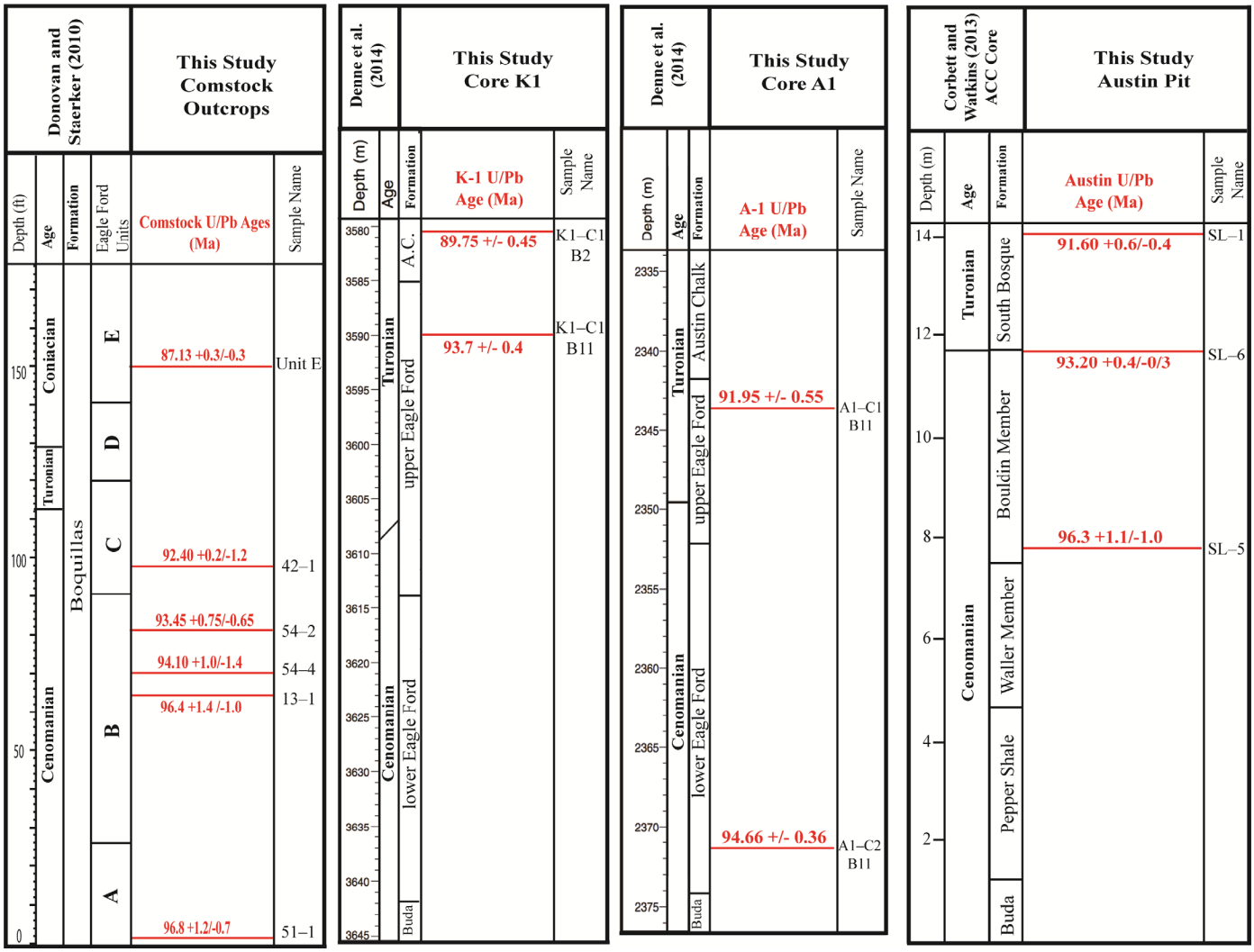


**Figure 11. Comparison of U–Pb ages with biozonations defined by Donovan and Staerker (2010), Corbett and Watkins (2013), and Denne et al. (2014) for the three areas of study. Red text indicates U–Pb ages obtained from this study, while black represents relative age assignments from these previous studies.**

fall stratigraphically within the uppermost samples interpreted by Donovan and Staerker (2010), indicating a late Cenomanian age. An ash bed (Boquillas Fm, sample 54–4) from 74 feet above the Buda–Eagle Ford contact, yielded an age of 94.1 +1.0/-1.4 Ma, indicating a position at or near the C–T boundary, defined at 93.9 Ma (Meyers et al., 2012). The biostratigraphic findings of (Donovan and Staerker, 2010) are consistent with this study's U–Pb age, which establishes this interval as late Cenomanian in age. The interval of youngest Cenomanian strata at this site was sampled 88 feet above the Buda–Eagle Ford contact. This ash bed (Boquillas Formation, sample 54–2) yielded an age of 93.45 +0.75/-0.65 Ma, indicating strata close to the C–T boundary or of early Turonian age. The lower-upper Eagle Ford boundary denoted as the unit B–C contact is interpreted to represent the transition from Cenomanian to Turonian strata based on biostratigraphy (Donovan and Staerker, 2010). These authors interpreted unit C to be early Turonian in age (Donovan and Staerker, 2010). Age dates obtained from an ash bed in the Boquillas Fm 8 feet above the unit B–C contact (92.4 +0.2/-1.2 Ma,) are in agreement with their biostratigraphically determined relative age of early Turonian. The ash bed at 9 feet below the Austin Chalk contact in unit E (Boquillas Formation, sample unit E), was dated 87.13 ± 0.3 Ma, in agreement with the biostratigraphic interpretations by Donovan and Staerker (2010) that all of unit E is Coniacian in age. In general, U–Pb ages determined in this study are consistent with relative ages determined from biostratigraphy with one exception being the upper part of unit B where U–Pb data indicate an early Turonian age (93.45 +0.75/-0.65 Ma) instead of the late Cenomanian age assigned by Donovan and Staerker (2010).

### Subsurface Core Comparisons

Two of the cores sampled for this study (A1 and K1) (Fig. 3) were characterized biostratigraphically by Denne et al. (2014). These cores provide an excellent opportunity to compare the U–Pb age's determinations obtained in the current study with biozonations.

Our age date of 91.95 ±0.55 Ma near the Eagle Ford–Austin Chalk boundary (sample A1–C1B11) (Figs. 8 and 11) indicates strata of middle/late Turonian age. This is supported by the placement of the C–T boundary 19 feet downsection based on faunal data by Denne et al. (2014). The age of 94.66 ± 0.36 Ma obtained near the base of the Eagle Ford Formation (sample A1–C2B11) in core A1, is significant given the high precision and resolution of this date and with little indication of Pb loss or inheritance. This younger age indicates a delayed onset of Eagle Ford deposition further demonstrating the variability of the Eagle Ford duration.

The biostratigraphic placement of the C–T boundary by Denne et al. (2014) in the K1 core is lower in the section than is suggested by results from ash U–Pb dates. Our sample from the upper Eagle Ford in this core (K1–C1B11) provided an age of 93.7 ± 0.4 Ma, which is within the accepted age range for the C–T boundary. Note that the C–T boundary in the K1 core, as defined by biostratigraphic data by Denne et al. (2014), occurs within the middle portion of the upper Eagle Ford, whereas the C–T boundary in the A1 core, is near the base of the upper Eagle Ford. This U–Pb age date is in minor disagreement with results from biostratigraphic findings. While the ash bed sample yielded a date with little evidence of Pb loss or common Pb, the older than expected age could be due to the population being affected by inheritance.

## Regional Correlation Framework

Correlation of Eagle Ford facies and stratigraphy from the outcrop belt to the South Texas subsurface in the oil and gas producing area has been attempted by several groups over the past few years (e.g., Donovan et al., 2012). This work has largely been based on lithostratigraphic correlations based on wireline logs and the assumption that they can be used to define chronostratigraphy.

Eldrett et al. (2014) argued that four ash beds from the Western Interior Seaway (A–D), as characterized by Elder (1988), can be correlated southward into the Maverick Basin. These correlations are not plausible for several reasons. First, observations made in Comstock area outcrops (Frebourg et al., 2016) and at the Austin pit locality show that individual ash beds are highly discontinuous locally. Second, as shown in this study, the chemical signatures of individual ash beds are not sufficiently unique to demonstrate continuity or correlatability. Rather, they suggest multiple volcanic sources were involved. Third, no geochronologic dates, no matter what method used, have high enough resolution to resolve individual beds considering their abundance and close spacing. The U–Pb ages of this study indicate that significant variation in duration of deposition exists within the Eagle Ford regionally. Although ash beds may be found in stratigraphically similar positions, chronostratigraphy does not support simple correlation of these beds over distances based on lithostratigraphic observations alone.

The Austin sample site, located near the San Marcos Arch (Fig. 3), represents the thinnest accumulation of Eagle Ford facies in the study. Compared with the Comstock area and the subsurface, Eagle Ford strata here contain fewer ash beds (Fig. 12). Only 8 ash beds were observed at the excavation pit in the Bouldin and South Bosque formations. Fairbanks (2012) and Fairbanks et al. (2016) showed that the underlying Waller Member and Pepper Shale are largely devoid of ash beds. Local correlation of thicker ash beds is possible as demonstrated by Fairbanks (2012) and Fairbanks et al. (2016), but regional correlation into the subsurface in South Texas is unlikely as determined by this study. Inhibiting factors with correlation of the ash beds include, bottom current reworking, bioturbation, erosion, and the limited original areal distribution of ash falls from each volcanic source region. The best example of this is the Bouldin Member, which totals 9 feet of section, but appears to account for 3.1 million years of time based on ages of 96.3 +1.1/-1.0 Ma (sample SL–5) and 93.20 +0.4/-0.3 Ma (sample SL–6) (Fig. 10), making it a highly condensed section. This scale of condensed section was not observed anywhere else within the Eagle Ford in this study.

In the subsurface of Atascosa and Karnes counties, similar degrees of complexity occur. The best example of this is the comparison between cores K1 and K2 that lie only four miles apart from each other (Fig. 9). Correlation based upon ash beds would seem straightforward between two cores of such close proximity. However, ash bed ages determined from the upper Eagle Ford section in these cores argue against this. For example, one of the ash beds dated (upper Eagle Ford Formation, sample K1–C1B11) is not present in the K2 core. It is probable that this ash bed was subsequently eroded in the vicinity of core K2 indicating the likelihood of missing section due to ash beds depositing in a blanket fashion. The next examples are the two ash beds found at the base of the Austin Chalk (samples K2–C1B18 and K1–C1B2). These are likely the same ash bed and have ages that are very similar (89.5 and 89.75 Ma) and have similar zircon population traits. However, gamma ray log responses from these wells suggest they are different (Figs. 5 and 12). These two ash beds are apparently absent in the A1 core, located only ~25 miles to the northwest (Fig. 9). Fairbanks (2012; Fairbanks et al., 2016) documented similar discontinuities of thick ash beds approximately 10 miles apart in the Austin area, and interpreted these to be due to local erosional events as have been documented in the Austin pit location and in West Texas outcrops (Frebourg et al., 2016). Bottom current reworking could provide a feasible explanation as to why the ash is not present in the A1 core, but the ash bed is upwards of 10 inches thick and second thickest in the study indicating a larger erosional process was active. If the second thickest ash bed found in the study cannot be correlated approximately 20 miles, it seems improbably that a thin ash bed as documented by Elder (1988) and Eldrett et al. (2015a) could be correlated with any degree of certainty.

Although not sampled in this study, the cores described by Fry (2015) from Zavala and Maverick counties (Fig. 3) display ash bed abundances far greater than those in cores studied herein. With abundant ash beds in both cores (170 in the Z1 core and 300 plus in the C1 core), correlation of at least the thicker beds might seem straightforward. Major ash beds identified in core by Eldrett et al. (2014) are not found to correlate to either the Zavala or Maverick county cores (Fry, 2015). Additionally, the thick ash beds found in the Comstock area outcrops, or the Lozier Canyon outcrops are not present (Fry, 2015).

The U–Pb ages generated in this study indicate regional chronostratigraphic correlations of major boundaries with and bounding the Eagle Ford Shale are not reliable. The base of the Eagle Ford in the Comstock outcrops is defined by an age of 96.8 +1.2/-0.7 Ma (Figs. 7 and 12). This age is in agreement with results generated from the core studied by Eldrett et al. (2014, 2015a), in Kinney County. In the A1 core, the ash bed located just above the contact with the Buda has an age of 94.66 ± 0.36 Ma. This age represents a difference of nearly 2.2 million years compared to the age of 96.8 +1.2/-0.7 Ma obtained from the base at the Comstock area outcrops. This is evidence that differential accommodation plays a significant role in the timing and duration of Eagle Ford strata across the basin. While no ash beds were recovered at the base of the Eagle Ford in Austin area, one ash bed was dated at 96.3 +1.1/-1.0 Ma (Fig. 10), indicating a contact with the Buda much older than the 96.8 +1.2/-0.7 Ma age observed in the Comstock area.

The age of the Eagle Ford–Austin Chalk contact is well constrained by the new U–Pb data presented in each of the study areas. The contact was previously considered to occur at the end of the Turonian (Jiang, 1989). More recently, Donovan and Staerker (2010) interpreted it to be in the lower Coniacian in Lozier Canyon. Data presented here show that in the Austin area, the contact is at roughly 91 Ma, still within the late Turonian. In cores K1 and K2, the contact can be interpreted to have an age of about 90 Ma based on ash beds (Fig. 9) near the Turonian-Coniacian boundary in the lower portion of the Austin Chalk. The age of an ash bed in the upper Eagle Ford of core A1 indicates middle Turonian age. Eldrett et al. (2014) interpreted the Austin Chalk contact at approximately 90.5 Ma, based upon palynological data. The largest variation in the ages assigned to the top of the Eagle Ford is between outcrops sampled in this study along U.S. highway 90 west of Comstock and those in Lozier Canyon. The ash bed (Fig. 8) near the Austin Chalk contact near Lozier Canyon was dated indicating a Coniacian age.

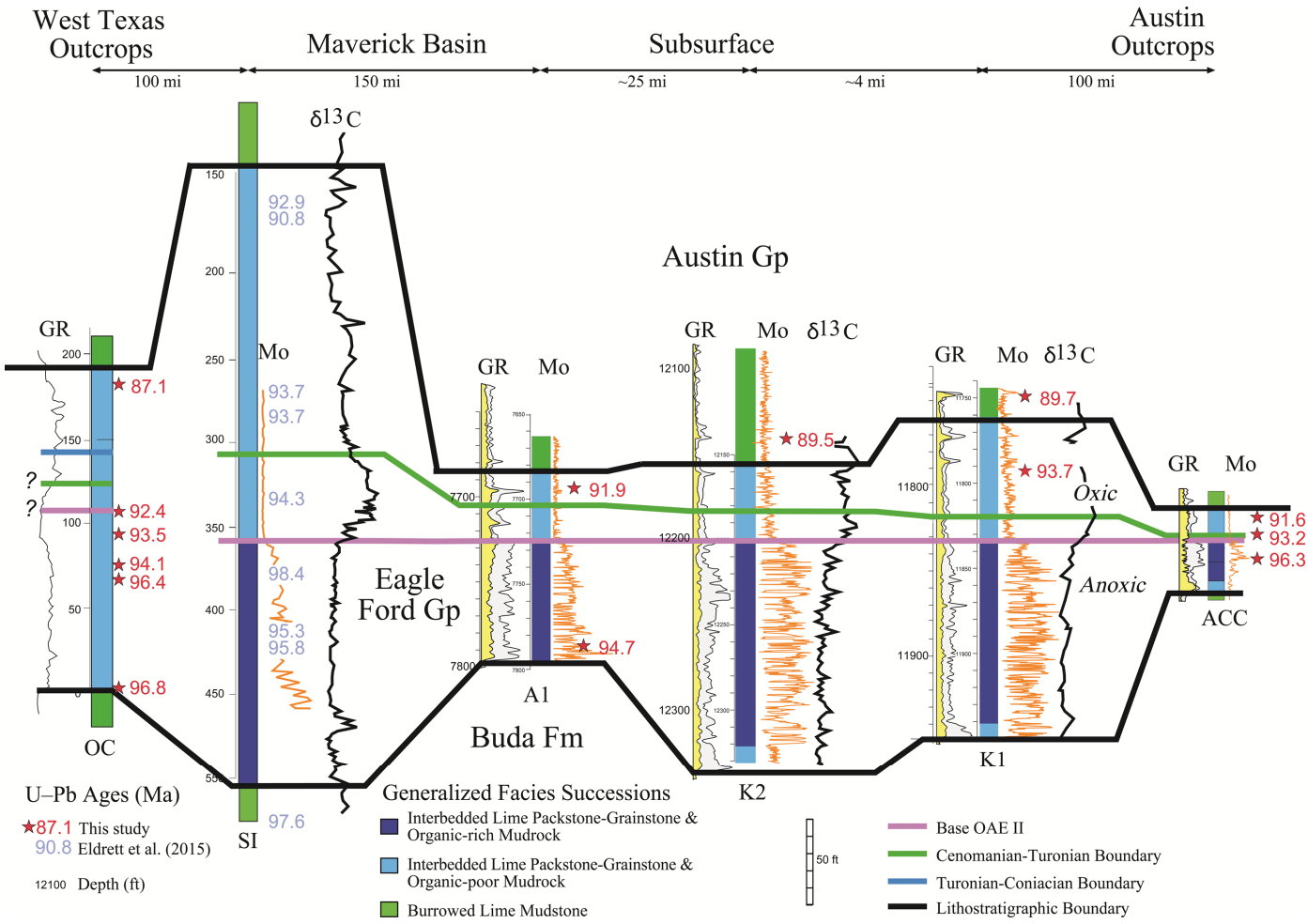


**Figure 12. Regional cross section of outcrops and subsurface cored wells characterized by chemostratigraphic and biostratigraphic methods in this study and by Eldrett et al. (2014, 2015a), Donovan et al. (2012), and Denne et al. (2014). U–Pb age data for this study labeled in red, with age data from Eldrett is labeled in blue. Datum is the OAE II.**

Biostratigraphic studies at Lozier Canyon also placed the contact in the lower Coniacian (Fig. 11) (Donovan and Staerker, 2010).

As indicated by this study's ash bed age dates, the large variations in sediment deposition of Eagle Ford across the study area is clearly, in part, due to local variations in accommodation, facies development, and/or erosion. This is likely the result of geographic variations in subsidence rate. In the subsurface, a number of faults are present and can partially explain thickness variations in a local setting (Denne et al., 2014). These bathymetric highs and lows can explain variation in the thickness of the Eagle Ford, while subsidence rate was key to the variability with the basal contact with the Buda. Denne et al. (2014) argued that erosion was prevalent at the lower-upper Eagle Ford contact. The top of the Eagle Ford at the contact with Austin Chalk has been locally truncated by erosion. The Eagle Ford–Austin Chalk boundary resulted from a change in ocean chemistry and a decrease in clay mineral rich sediment input. This can be observed through decreasing gamma ray values, increased benthic fauna, and a reduction of total organic carbon (TOC) in the system. Additionally, the basal Austin Chalk contact varies laterally with previous studies suggesting both unconformable and conformable contacts with the Eagle Ford (Passagno, 1969; Sohl et al., 1991; Manicini and Puckett, 2005). This suggests differential accommodation contributing to the variation in ages at the Eagle Ford–Austin Chalk contact. Increased oxygenation of bottom waters began around the lower-upper Eagle Ford contact as evidenced by lower concentrations of redox sensitive elements, as well as the presence of burrows and benthic forams. Above the lower-upper Eagle Ford contact, no well-developed oxygen minimum zone was present on the South Texas Shelf based upon reduction in redox sensitive elements and the occurrence of benthic fauna (Donovan et al., 2012; Denne et al., 2014). Detrital clay mineral input into the system began to decrease first in the areas of the Austin and subsurface cores potentially indicating a clay mineral source more proximal to the Comstock outcrop area. This allowed the system to support the burrowing fauna of the Austin Chalk, while areas more proximal to argillaceous sediment provenance (Comstock area/Lozier Canyon) continued depositing clay-rich Eagle Ford facies (Hentz and Ruppel, 2010; Frebourg et al., 2016). This change to Austin Chalk type facies occurred upwards of 4.5 million years later in the Comstock area/Lozier Canyon (Fig. 12). It was not until clay mineral input was reduced and increased oxygenation of the water column occurred that Eagle Ford facies deposition ceased. This variation in age of the Eagle Ford–Austin Chalk contact proves that the conventional chronostratigraphic interpretation of this contact was incorrect and that it is instead a time transgressive boundary. With U–Pb age data, new chemostratigraphy, and recent biostratigraphic data from Donovan et al. (2012) and Denne et al. (2014), it can be concluded that the Eagle Ford–Austin Chalk contact varies in age greatly across the basin.

## CONCLUSIONS

Study of the prevalent volcanic ash beds preserved within the Eagle Ford has led to a more complete understanding of the complexity and heterogeneities observed within this South Texas formation. $^{206}Pb/^{238}U$ ages derived by laser-ablation analysis of zircons in these beds at three separate study locations across South Texas demonstrate distinct differences in the time intervals during which Eagle Ford rocks were deposited. New ash bed dates from the base of Eagle Ford–equivalent Boquillas outcrops in the Comstock area in West Texas indicate that deposition there began at about 97 Ma during the early Cenomanian. In contrast, dates from near the base of the Eagle Ford in subsurface core in Atascosa County, show that Eagle Ford deposition there began much later at about 94.66 Ma in the middle to late Cenomanian. The end of Eagle Ford deposition in the Comstock area occurred at about 87 Ma in the Coniacian, but in Karnes County, on the Central Texas shelf, good evidence of erosion is present making it difficult to know exactly when deposition ceased. If erosion was only minor, the transition to Austin Chalk facies appears to have happened much earlier in the late Turonian at about 90 Ma. Finally, in the vicinity of Austin, faunal studies and ash bed dating from this study show that the top of the Eagle Ford in this area is of middle to late Turonian age (approximately 91 Ma). These results demonstrate regional variation in the ages of the top and bottom of Eagle Ford deposition. Exact durations of deposition are hampered by both local and regional variations in erosion. Causes for variable ages for the onset of Eagle Ford deposition in Atascosa County is interpreted to be largely driven by inherited paleobaythmetric highs and differences in relative subsidence.

The new U–Pb ages documented in this study provide insights into the ability to correlate ash beds. Observations made from outcrop show finite potential to correlate single ash beds locally along adjacent road cuts. In the subsurface, prominent thick ash beds can sometimes be correlated between extremely proximal cores. However, as distance increases, reliability of correlation decreases as demonstrated by the absence of the upper most ash in the A1 core that is present in both the K1 and K2 cores. Because data show that correlations of individual, or even groups of ash beds from outcrops to the subsurface are in almost all cases improbable, such correlations should not be considered valid for lithostratigraphic or chronostratigraphic correlations at even small scales.

The U–Pb geochronologic work from this study places important age constraints on proposed relative ages from biostratigraphic findings in the Comstock, subsurface, and Austin areas. In the Comstock area and in Austin, U–Pb ages are, in large part, in line with other proposed ages for the C–T boundary in other areas of the Western Interior Seaway and are within the uncertainties proposed for the GSSP by Meyers et al. (2012).

Determining the exact sources of the volcanic ash deposits remains challenging because of the varying levels of alteration that has affected the ash beds. It can be concluded that the ash beds of the Eagle Ford represent volcanic material from multiple sources. The andesitic through rhyolitic compositions displayed by some ash beds indicate compositions that are typical of arc volcanism, similar to that which could have origins in northern Mexico and southern Arizona. The ultrabasic foidite and basalts have compositionally similar silica weight percentages with that of the local Balcones Igneous Province. Additionally, the similarity in xenocryst ages and increasing abundance of ash beds near the Balcones Igneous Province indicate a probable connection to these eruptive sources. When factoring in the distance that ashes can travel, the thickness of ash deposits, paleowind direction, composition, xenocryst ages, and zircon size, the arc volcanism of northern Mexico and the Balcones Igneous Province of Central Texas are the two most probable source regions for many of the ash beds preserved in Eagle Ford and sub/superjacent strata.

## ACKNOWLEDGMENTS

Support for this project was provided by the members of the Mudrock System Research Laboratory (MSRL) Consortium. These members include Anadarko, Apache, BP, Centrica, Cenovus, Chesapeake, Cima, Cimarex, Chevron, Concho, ConocoPhilips, Cypress, Devon, Encana, ENI, EOG, EXCO, ExxonMobil, Hess, Husky, IMP, Kerogen, Marathon, Murphy, Newfield, Penn West, Penn Virginia, Pioneer, Samson, Shell, StatOil, Talisman, Texas American Resources, The Unconventionals, US EnerCorp, Valence, and YPF.

Lisa Stockli for teaching me everything about running the laser; the first author thanks professors Stephen Ruppel, Harry Rowe, Danny Stockli, Bill Fisher, Roland Mundil, and Paul Renne for sharing their wealth of knowledge; and the Berkeley Geochronology Center for allowing the use of their facilities on numerous occasions. The first author would also like to thank Shanley Chien for her help in the editing process. Finally, the first author would like to thank his fellow MSRL cohorts, friends, and—most importantly—his family for their constant love and support.

The work detailed in this paper is based on of the Master's thesis work completed by John Pierce at the University of Texas, at Austin. Publication authorized by the Director, Bureau of Economic Geology, Austin, Texas.

## REFERENCES CITED

Alexandre, J. T., E. Tuenter, G. A. Henstra, K. J. van der Zwan, R. S. van de Wal, H. A. Dijkstra, and P. L. de Boer, 2010, The mid-Cretaceous North Atlantic nutrient trap: Black shales and OAEs: Paleoceanography, v. 25, PA4201, p. 1–14.

Armstrong, R. L., W. H. Taubeneck, and P. O. Hales, 1977, Rb–Sr and K–Ar geochronometry of Mesozoic granitic rocks and their Sr isotopic composition, Oregon, Washington, and Idaho: Geological Society of America Bulletin, v. 88, p. 397–411.

Baldwin, O. D., and J. A. S. Adams, 1971, $^{40}K/^{39}Ar$ Ages of the alkaline igneous rocks of the Balcones Fault trend of Texas: Texas Journal of Science, v. 22, p. 223–231.

Barker, D. S., 1996, Nephelinite-phonolite volcanism, *in* R. H. Mitchell, ed. Undersaturated alkaline rocks: Mineralogy, petrogenesis, and economic potential: Mineralogical Association of Canada Short Course Series 24, Quebec City, Quebec, p. 23–44.

Blakey, R., 2013, Western North American series: <http://www.cpgeosystems.com/paleomaps.html> Accessed May 2013.

Cardin, A. A. J., T. K. Kyser, W. G. E. Caldwell, and F. J. Longstaffe, 1995, Isotopic and chemical compositions of bentonites as paleoenvironmental indicators of the Cretaceous Western Interior Seaway: Paleogeography, Paleoclimatology, Paleoecology, v. 119, p. 301–320.

Centeno-García, E., M. Guerrero-Suastegui, and O. Talavera-Medoza, 2008, The Guerrero Composite Terrane of western Mexico: Collision and subsequent rifting in a supra-subduction zone: Geological Society of America Special Paper 436, Boulder, Colorado, p. 279–308.

Cobban, W. A., S. C. Hook, and K. C. McKinney, 2008, Upper Cretaceous molluscan record along a transect from Virden, New Mexico, to Del Rio, Texas: New Mexico Geology, v. 30, p. 75–92.

Corbett, M. J., and D. K. Watkins, 2013, Calcareous nannofossil paleoecology of the mid-Cretaceous Western Interior Seaway and evidence of oligotrophic surface waters during OAE2: Palaeogeography, Palaeoclimatology, Palaeoecology, v. 392, p. 510–523.

Denne, R. A., R. E. Hinote, J. A. Breyer, T. H. Kosanke, J. A. Lees, N. Engelhardt-Moore, J. M. Spaw, and N. Tur, 2014, The Cenomanian-Turonian Eagle Ford Group of South Texas: Insights on timing and paleoceanographic conditions from geochemistry

and micropaleontologic analyses: Palaeogeography, Palaeoclimatology, Palaeoecology, v. 413, p. 2–28.

Donovan, A. D., and T. S. Staerker, 2010, Sequence stratigraphy of the Eagle Ford (Boquillas) Formation in the subsurface of South Texas and outcrops of West Texas: Gulf Coast Association of Geological Societies Transactions, v. 60, p. 181–190.

Donovan, A. D., T. S. Staerker, A. Pramudito, W. Li, M. J. Corbett, C. M. Lowery, A. M. Romero, and R. D. Gardner, 2012, The Eagle Ford outcrops of West Texas: A laboratory for understanding heterogeneities within unconventional mudstone reservoirs: Gulf Coast Association of Geological Societies Journal, v. 1, p. 162–185.

Dunn, D. P., 2002, Xenolith mineralogy and geology of the Prairie Creek Lamproite Province, Arkansas: Ph.D. Dissertation, University of Texas at Austin, 160 p.

Elder, W. P., 1987, Cenomanian-Turonian (Cretaceous) stage boundary extinctions in the Western Interior of the United States: Ph.D. Dissertation, University of Colorado, Boulder, 621 p.

Elder, W. P., 1988, Geometry of Upper Cretaceous bentonite beds: Implications about volcanic source areas and paleowind patterns, Western Interior, United States: Geology, v. 16, p. 835–838.

Elder, W. P., 1991, Molluscan paleoecology and sedimentation patterns of the Cenomanian-Turonian extinction interval in the southern Colorado Plateau region, *in* J. D. Nations and J. G. Eaton, eds., Stratigraphy, depositional environments, and sedimentary tectonics of the western margin, Cretaceous Western Interior Seaway: Geological Society of America Special Paper 260, Boulder, Colorado, p. 113–137.

Eldrett, J. S., D. Minisini, and S. C. Bergman, 2014, Decoupling of the carbon cycle during Ocean Anoxic Event 2: Geology, v. 42, p. 567–570.

Eldrett, J. S., C. Ma, S. C. Bergman, B. Lutz, F. J. Gregory, P. Dodsworth, M. Phipps, P. Hardas, D. Minisini, A. Ozkan, J. Ramezani, S. A. Bowring, S. L. Kamo, K. Ferguson, C. Macaulay, and A. E. Kelly, 2015a, An astronomically calibrated stratigraphy of the Cenomanian, Turonian and earliest Coniacian from the Cretaceous Western Interior Seaway, USA: Implications for global chronostratigraphy: Cretaceous Research v. 56, p. 316–344.

Eldrett, J. S., C. Ma, S. C. Bergman, A. Ozkan, D. Minisini, B. Lutz, S.-J. Jackett, C. Macaulay, and A. E. Kelly, 2015b, Origin of limestone–marlstone cycles: Astronomic forcing of organic-rich sedimentary rocks from the Cenomanian to Early Coniacian of the Cretaceous Western Interior Seaway, USA: Earth and Planetary Science Letters, v. 423. p. 98–113

Erba, E., 2004, Calcareous nannofossils and Mesozoic oceanic anoxic events: Marine Micropaleontology, v. 52, p. 85–106.

Ewing, T. E., and C. S. Caren, 1982, Late Cretaceous volcanism in south and Central Texas: Stratigraphic, structural, and seismic models: Gulf Coast Association of Geological Societies Transactions, v. 32, p. 137–145.

Fairbanks, M. D., 2012, High-resolution stratigraphy and facies architecture of the upper Cretaceous (Cenomanian-Turonian) Eagle Ford Group, Central Texas: Master's Thesis, University of Texas at Austin, 129 p.

Fairbanks, M. D., S. C. Ruppel, and H. Rowe, 2016,, High resolution stratigraphy and facies architecture of the Upper Cretaceous (Cenomanian-Turonian) Eagle Ford Group, Central Texas: American Association of Petroleum Geologists Bulletin, v. 100, p. 379–403.

Frébourg, G., S. C. Ruppel, R. G. Loucks, and J. Lambert, 2016, Depositional controls on sediment body architecture in the Eagle Ford/Boquillas system: Insights from outcrops in West Texas, USA: American Association of Petroleum Geologists Bulletin, v. 100, p. 657–682.

Fry, K. O., 2015, Lithofacies, Bbiostratigraphy, chemostratigraphy, and stratal architecture of the Boquillas Formation and Eagle Ford Group: A comparison of outcrop and core data from Big Bend National Park to Maverick Basin, Southwest Texas, USA: Master's Thesis, University of Texas at Austin, 253 p.

Galloway, W. E., 2008, Depositional evolution of the Gulf of Mexico sedimentary basin, *in* A. D. Miall, eds., The sedimentary basins of the United States and Canada: Elsevier, New York, New York, 610 p.

Gill, J. R., and W. A. Coban, 1973, Stratigraphy and geologic history of the Montana Group, and equivalent rocks, Montana, Wyoming, and North and South Dakota: U.S. Geological Survey Professional Paper 776, p. 37.

Gleason, J. D., G. E. Gehrels, W. R. Dickinson, P. J. Patchett, and D. A. Kring, 2007, Laurentian sources for detrital zircon grains in turbidite and deltaic sandstones of the Pennsylvanian Haymond Formation, Marathon assemblage, West Texas, USA: Journal of Sedimentary Research, v. 77, p. 888–900.

Gonzalez-Mellado, A. O., and S. de la Cruz-Reyna, 2010, A simple semi-empirical approach to model thickness of ash-deposits for different eruption scenarios: Natural Hazards and Earth System Sciences, v. 10, p. 2241–2257.

Gradstein, F. M., J. G. Ogg, M. D. Schmitz, and G. Ogg, 2012, The geologic time scale 2012: Elsevier, Boston, Massachusetts, 1176 p.

Griffin, W. R., 2008, Geochemistry and geochronology of the Balcones Igneous Province, Texas: Ph.D. Dissertation, University of Texas at Dallas, 241 p.

Griffin, W. R., K. A. Foland, J. R. Stern, and M. I. Leybourne, 2010, Geochronology of bimodal alkaline volcanism in the Balcones Igneous Province, Texas: Implications for Cretaceous intraplate magmatism in the northern Gulf of Mexico magmatic zone: Journal of Geology, v. 118, p. 1–21.

Hasegawa, H., R. Tada, X. Jiang, Y. Suganuma, S. Imsamut, P. Charusiri, N. Ichinnorov, and Y. Khand, 2012, Drastic shrinking of the Hadley circulation during the mid-Cretaceous supergreenhouse: Climate Past, v. 8, p. 1323–1337.

Hazzard, R. T., 1959, Measured section, *in* Geology of the Val Verde Basin: West Texas Geological Society Guidebook, Midland, 118 p.

Hentz, T. F., and S. C. Ruppel, 2010, Regional lithostratigraphy of the Eagle Ford Shale: Maverick Basin to East Texas Basin: Gulf Coast Association of Geological Societies Transactions, v. 60, p. 325–337.

Horstwood, M. S. A., 2008, Data reduction strategies, uncertainty assessment and resolution of LA–(MC–)ICP–MS isotope data, *in* P. J. Sylvester, ed., Laser ablation ICP–MS in the Earth Sciences: Current practices and outstanding issues: Mineralogical Association of Canada Short Course Series 40, Quebec City, Quebec, p. 283–303.

Hunter, B. E., and D. K. Davies, , 1979, Distribution of volcanic sediments in the Gulf Coastal Province—Significance to petroleum geology: Gulf Coast Association of Geological Societies Transactions, v. 29, p. 147–155.

Jackson, S. E., N. J. Pearson, W. L. Griffin, and E. A. Belousova, 2004, The application of laser ablation-inductively coupled plasma-mass spectrometry to in situ U–Pb zircon geochronology: Chemical Geology, v. 211, p. 47–69.

Jiang, M., 1989, Biostratigraphy and geochronology of the Eagle Ford Shale, Austin Chalk, and the lower Taylor Marl in Texas based on calcareous nannofossils: Ph.D. Dissertation, Texas A&M University, College Station, 524 p.

Kennedy, W. J., I. Walaszczyk, and W. A. Cobban, 2005, The global boundary stratotype section and point for the base of the Turonian Stage of the Cretaceous; Pueblo, Colorado, USA: Episodes, v. 28, no. 2, p. 93–104.

Kirkland, J. I., 1991, Lithostratigraphic and biostratigraphic framework for the Mancos Shale (late Cenomanian to middle Turonian) at Black Mesa, northeastern Arizona, *in* J. D. Nations and J. G. Eaton, eds., Stratigraphy, depositional environments, and sedimentary tectonics of the western margin, Cretaceous Western Interior Seaway: Geological Society of America Special Paper 260, Boulder, Colorado, p. 85–111.

Leckie, R. M., T. J. Bralower, and R. Cashman, , 2002, Oceanic anoxic events and plankton evolution: Biotic response to tectonic forcing during the mid-Cretaceous: Paleoceanography, v. 17, p. 1–29

Ludwig, K. R., 1991, ISOPLOT—A plotting and regression program for radiogenic-isotope data: U.S. Geological Survey Open-File Report 91–445, 39 p.

Lundquist, J. J., 2000, Foraminiferal biostratigraphic and paleoceanographic analysis of the Eagle Ford, Austin, and lower Taylor Groups (middle Cenomanian through lower Campanian) of Central Texas: Ph.D. Dissertation, University of Texas at Austin, 545 p.

Ma, C., S. R. Meyers, B. B. Sageman, B. S. Singer, and B. R. Jicha, 2014, Testing the astronomical time scale for Oceanic Anoxic Event 2, and its extension into the Cenomanian Strata of the Western Interior Basin (USA): Geological Society of America Bulletin, v. 126, p. 974–989.

Mahoney, J. J., M. Storey, R. A. Duncan, K. J. Spencer, and M. Pringle, 1993, Geochemistry and age of Ontong Java Plateau, *in* M. Pringle, W. W. Sager, W. V. Sliter, and S. Stein, eds. The Mesozoic Pacific geology, tectonics, and volcanism: American Geophysical Union, Washington, D.C., p. 233–261

Mancini, E. A., and T. M. Puckett, 2005, Jurassic and Cretaceous transgressive-regressive (TR) cycles, northern Gulf of Mexico, USA: Stratigraphy, v. 2, p. 31–48.

Mastin, L. G., M. Guffanti, R. Servranckx, P. Webley, S. Barsotti, K. Dean, A. Durant, J. W. Ewert, A. Neri, W. I. Rose, D. Schneider, L. Siebert, B. Stunder, G. Swanson, A. Tupper, A. Volentik, and C. F. Waythomas, 2009, A multidisciplinary effort to assign realistic source parameters to models of volcanic ash cloud transport and dispersion during eruptions: Journal of Volcanology and Geothermal Research, v. 186, p. 10–21.

McDonough, W. F., and S. Sun, 1995, The composition of the Earth: Chemical Geology, v. 120, p. 223–253.

McDowell, F. W., J. Roldán-Quintana, and J. N. Connelly, 2001, Duration of Late Cretaceous–Early Tertiary magmatism in east-central Sonora, Mexico: Geological Society of America Bulletin, v. 113, p. 521–531.

Meyers, S. R., S. E. Siewert, B. S. Singer, B. B. Sageman, D. J. Condon, J. D. Obradovich, B. R. Jicha, and D. A. Sawyer, 2012, Intercalibration of radioisotopic and astrochonologic time scales for the Cenomanian-Turonian boundary interval, Western Interior Basin, USA: Geology, v. 40, no. 1, p. 7–10.

Miggins, D. P., C. D. Blome, and D. V. Smith, 2004, Preliminary $^{40}Ar/^{39}Ar$ geochronology of igneous intrusions from Uvalde County, Texas: Defining a more precise eruption history for the southern Balcones Volcanic Province: U.S. Geological Survey Open-File Report 2004–1031, 33 p.

Obradovich, J., 1993, A Cretaceous time scale, *in* W. G. E. Caldwell and E. G. Kauffman, eds. Evolution of the Western Interior Basin: Geological Society of Canada Special Paper 39, St. John's, Newfoundland, p. 379–396.

Passagno, E. A., 1969, Upper Cretaceous stratigraphy of the western Gulf Coast area of Mexico, Texas, and Arkansas: Geological Society of America Memoir 111, Boulder, Colorado, p. 1–139.

Phelps, R. M., 2011, Middle-Hauterivian to lower-Campanian sequence stratigraphy and stable isotope geochemistry of the Comanche Platform, South Texas: Ph.D. Dissertation, University of Texas at Austin, 240 p.

Pyle, D. M., 1989, The thickness, volume and grainsize of tephra fall deposits: Bulletin of Volcanology, v. 51, p. 1–15.

Ramana, M. V., T. Ramprasad, and M. Desa, 2001, Seafloor spreading magnetic anomalies in the Enderby Basin, East Antarctica: Earth and Planetary Science Letters., v.191, p. 241–255.

Roberts, L. N. R., and M. A. Kirschbaum, 1995, Paleogeography of the Late Cretaceous of the Western Interior of middle North America—Coal distribution and sediment accumulation: U.S. Geological Survey Professional Paper 1561, p. 1–115.

Ross, C. S., H. D. Miser, and L. W. Stephenson, 1929, Water-laid volcanic rocks of early Upper Cretaceous age in southwestern Arkansas, southeastern Oklahoma, and northeastern Texas: U.S. Geological Survey Professional Paper 154–F, p. 175–202.

Rowe, H., N. Hughes, and K. Robinson, 2012, The quantification and application of handheld energy-dispersive X-ray fluorescence (ED–XRF) in mudrock chemostratigraphy and geochemistry: Chemical Geology, v. 324–325, p. 122–131.

Ruppel, S. C., R. G. Loucks, and G. Frébourg, 2013, Guide to the exposures of the Eagle Ford–Equivalent Boquillas Formation and related upper Cretaceous units in Southwest Texas: Bureau of Economic Geology, Mudrock Systems Research Laboratory, Field Trip Guide, Austin, 151 p.

Sageman, B. B., B. S. Singer, S. R. Meyers, S. E. Siewert, I. Walaszczyk, D. J. Condon, B. R. Jicha, J. D. Obradovich, and D. A. Sawyer, 2014, Integrating $^{40}Ar/^{39}Ar$, U–Pb, and astronomical clocks in the Cretaceous Niobrara Formation, Western Interior Basin, USA: Geological Society of America Bulletin, v. 126, p. 956–973.

Schoene, B., C. Latkoczy, U. Schaltegger, and D. Gunther, 2010, A new method integrating high-precision U–Pb geochronology with zircon trace element analysis (U–Pb TIMS–TEA): *Geochimica et Cosmochimica Acta*, v. 74, p. 7144–7159.

Silver, L. T., T. H. Anderson, and B. W. Chappell, 1993, The Cretaceous batholiths of "greater" Sonora, *in* C. Gonzalez-Leen and E. L. V. Granillo, eds., *Resumenes del III Simpósio de la Geología de Sonora y areas adyacentes*: National Autonomous University of Mexico and University of Sonora, March, Hermosillo, Sonora, March 28–31, p. 114-115.

Sinton, C. W., and R. A. Duncan, 1997, Potential links between ocean plateau volcanism and global ocean anoxia at the Cenomanian-Turonian boundary: Economic Geology, v. 92, p. 836–842.

Sinton, C. W., R. A. Duncan, M. Storey, J. Lewis, and J. J. Estrada, 1998, An oceanic flood basalt province within the Caribbean Plate: Earth and Planetary Science Letters, v. 155, p. 221–235.

Slaughter, M., and M. Hamil, 1970, Model for deposition of volcanic ash and resulting bentonite: Geological Society of America Bulletin, v. 81, p. 961–968.

Smith, D. V., B. D. Smith, and P. L. Hill, 2002, Aeromagnetic survey of Medina and Uvalde counties, Texas: U.S. Geological Survey Open-File Report 02–49, 10 p.

Sohl, N. F., R. E. Martinez, P. Salmeron-Urena, and F. Soto-Jaramillo, 1991, Upper Cretaceous, *in* A. Salvador, ed., The geology of North America, v. J: The Gulf of Mexico Basin: Geological Society of America, Boulder, Colorado, p. 205–244.

Sparks, R. S. J., M. I. Bursik, G. J. Ablay, R. M. E. Thomas, and S. N. Carey, 1992, Sedimentation of tephra by volcanic plumes. Part 2: Controls on thickness and grain-size variations of tephra fall deposits: Bulletin of Volcanology, v. 52, p. 685–695.

Stott, D. F., 1963, The Cretaceous Alberta Group and equivalent rocks, Rocky Mountain Foothills, Alberta: Geological Survey of Canada Memoir 317, Calgary, Alberta, 306 p.

Storey, M., J. J. Mahoney, A. D. Saunders, R. A. Duncan, S. P. Kelley, and M. F. Coffin, 1995, Timing of hot spot related volcanism and the breakup of Madagascar and India: Science, v. 267, p. 852–855.

Surles, M. A., Jr., 1987, Stratigraphy of the Eagle Ford Group (Upper Cretaceous) and its source-rock potential in the East Texas Basin: Baylor Geological Studies Bulletin 45, Waco, Texas, 57 p.

Sylvester, P. J., 2008, LA–(MC–)ICP–MS trends in 2006 and 2007 with particular emphasis on measurement uncertainties: Geostandards and Geoanalytical Research, v. 32, p. 469–488.

Tejada, M. L. G., J. J. Mahoney, R. A. Duncan, and M. P. Hawkins, 1996, Age and geochemistry of basement and alkalic rocks of Malaita and Santa Isabel, Solomon Islands, southern margin of Ontong Java Plateau: Journal of Petrology, v. 37, p. 361–394.

Tera, F., and G. J. Wasserburg, 1972, U–Th–Pb systematics in three Apollo 14 basalts and the problem of initial Pb in lunar rocks: Earth and Planetary Science Letters v. 14, no. 3, p. 28–304.

Toth, M. I., 1985, Petrology and evolution of the Bitterroot lobe of the Idaho batholith: Geological Society of America Abstracts with Programs, v. 17, no. 4, p. 269.

Zartman, R. E., 1977, Geochronology of some alkali rock provinces in eastern and central United States: Annual Review of Earth and Planetary Sciences, v. 5, p. 257–286.